NONDESTRUCTIVE ON-LINE MEASUREMENT SYSTEM FOR *IN-VITRO* CELL PROLIFERATION IN MICRO-POROUS POLYMER SCAFFOLDS

Dariusz Dziong, B.Eng.

Department of Biomedical Engineering
Faculty of Medicine
McGill University
Montreal, Canada

A thesis submitted to the faculty of Graduate Studies and Research in partial fulfillment of the requirements of the degree of Master of Engineering

Your file Votre référence
ISBN: 978-0-494-24952-9
Our file Notre référence
ISBN: 978-0-494-24952-9

ABSTRACT

Tissue engineering requires diagnostic tools for *in-vitro* monitoring of cell proliferation in three-dimensional scaffolds. Current methods are inaccurate, prohibitively expensive, or compromise sample integrity. This work presents a nondestructive system for the on-line measurement of cell concentration in micro-porous polymer scaffolds. The system is based on measuring the reflection coefficient of the sample with an open-ended coaxial probe over a frequency range of 10-200 MHz. An aperture admittance model is used to extract the complex permittivity from the reflection measurement. Then, effective medium approximation is used to relate the complex permittivity to the cell properties and concentration of the sample.

The system detected the relative cell concentration differences between micro-porous polymer scaffolds seeded with progressively greater number of pre-osteoblast cells. Proliferation of pre-ostoblasts over 14 days was measured within 56 scaffolds by the system and a concurrent DNA assay. The recorded cell proliferation data corresponded well to each other and those found in literature. Thus, the system can be applied for on-line monitoring of cell proliferation within micro-porous polymer scaffolds.

RÉSUMÉ

Le génie tissulaire nécessite des outils diagnostiques pour le suivi *in-vitro* de la prolifération cellulaire au sein de supports de culture tridimensionnels. Les méthodes courantes sont imprécises, extrêmement coûteuses, ou encore compromettent l'intégrité de l échantillon. Ce travail présente un système non destructif pour la mesure en ligne de la concentration cellulaire dans des supports polymères microporeux. Le système est basé sur la mesure du coefficient de réflexion de l'échantillon, effectuée par l'intermédiaire d'une sonde coaxiale ouverte sur une gamme de fréquence de 10-200 mégahertz. Un modèle d'admittance est utilisé pour extraire la permittivité complexe à partir de la mesure de réflexion. Une approximation équivalente a été développée pour relier la permittivité complexe aux propriétés des cellules et à la concentration de l'échantillon.

Le système a permis de détecter les différences relatives de concentration cellulaire entre plusieurs supports polymères microporeux mises en culture avec un nombre croissant de cellules pré-ostéoblastiques. La prolifération des pré-ostéoblastes a été mesurée sur une période de 14 jours dans 56 supports à l'aide du système développé et d'un système concurrent de mesure de l'ADN. Les données de prolifération cellulaire enregistrées correspondent les unes aux autres ainsi qu'à celles trouvées dans la littérature.

ACKNOWLEDGEMENTS

I would like to express my gratitude to my supervisors Dr. Maryam Tabrizian and Dr. Robert Kearney and for their guidance, support, and for giving me the opportunity to work on an interesting and sophisticated research project. I am very much grateful for the freedom I was granted in regards to the direction of the project, as well as, for the opportunities and experiences that were presented to me by way of conferences and seminars made available by both supervisors.

My gratitude goes to Mr. Raymond Waterburry who was the greatest motivator in my broaching the graduate experience. I am appreciative for his suggestions, discussion, and constant support in all technical and literary matters. I would like to thank Dr. Pierre Bagnaninchi, who was the parent of this project, for his patience in the transfer of knowledge that transpired between us and for his continued guidance and interest in this research.

Given the multidisciplinary nature of this work numerous people must be acknowledged for their generosity in regards to equipment loan and access. I would like to thank: Dr. Teodor Veres for the Network Analyzer loan, Dr. Satya Prakash for granting me access to his centrifuge and freezer, Dr. Galiana for the data acquisition card loan, and Agilent Technologies for the loan of the impedance analyzer and for their thorough technical support.

Certain people were extraordinarily helpful in the progress of this work. In that vein, I would like to thank Mrs. Line Mongeon for performing all the scanning electron microscopy for this research. Similarly, I would like to thank Jean-Philippe St-Pierre for his guidance with cell-culture, DNA assay protocols and certain data analyses. Also, a special nod of gratitude goes to all the members of the biomaterials laboratory who helped me find my way around a wet lab.

The task of this research and degree was made that much more enjoyable and entertaining by two friends of mine Mr. Daniel Seliskar and Mr. Sasha Semienchuk who underwent the same ordeal at the same time. I would like to thank them both for their incessant camaraderie, help, and general support.

Last, I would like to thank my loving parents for always being there for me in all ways necessary and more.

This work was supported by funding provided by the Fonds Quebecois de la Recherche sur la Nature et les Technologies (FQRNT) and the Natural Sciences and Engineering Research Council (NSERC).

TABLE OF CONTENTS

LIST OF FIGURES

LIST OF TABLES

PREFACE

The one journal manuscript and one proceedings paper presented in this thesis were written by Dariusz Dziong in collaboration with Dr. Pierre Bagnaninchi, Dr. Maryam Tabrizian, and Dr. Robert Kearney. The actual experimentation, data acquisition, and data analysis were performed by Dariusz Dziong.

GLOSSARY OF TERMS

$\vec{D}$	Electric displacement field
$\vec{E}$	Electric field
$\vec{P}$	Polarization
ε	Permittivity (Absolute)
ε_0	Permittivity of free space
ε_r	Relative permittivity
ε_s	Static permittivity (relative)
ε_∞	Optic permittivity (relative)
ε^*	Complex permittivity (relative unless otherwise specified)
ε_m^*	Complex permittivity of ambient medium (relative)
ε_{mem}^*	Complex permittivity of cell membrane (relative)
ε_{cell}^*	Complex permittivity of cell (relative)
ε_{cyt}^*	Complex permittivity of cytoplasm (relative)
ε_{sample}^*	Complex permittivity of sample (relative)
ε_{ck}^*	Complex permittivity of the k^{th} inclusion (relative)
ε_{eff}^*	Complex effective permittivity (relative)
ε'	Real permittivity (relative)
$\varepsilon_{cyt}^{'}$	Real permittivity of cytoplasm (relative)
$\varepsilon_{mem}^{'}$	Real permittivity of cell membrane (relative)
ε_m	Real permittivity of ambient medium (absolute)
ε''	Imaginary permittivity (relative)
ε_l	Permittivity of dielectric in coaxial line (relative)
r_c	Outer radius of spherical cell model
d	Thickness of cell membrane for a spherical cell model
v	Volume factor $v = (1 - d / r_c)^3$
ω	Angular frequency

σ	Conductivity
σ_{cyt}	Cytoplasm conductivity
σ_S	Static conductivity
σ_D	Dynamic conductivity
∂	Loss angle
$\tan\partial$	Loss tangent
τ	Time constant
C_l	Fringe Capacitance
C_0	Capacitance proportional to sample permittivity
Y_L	Load admittance
j	Imaginary unit: $\sqrt{-1}$
$K_{i\,for\,I\,=\,1,2,3,4}$	Frequency dependant constants specific to coaxial probe geometry
a	Radius of inner coaxial conductor
b	Radius of outer coaxial conductor
k	Wavenumber
μ_0	Permeability of free space
r'	Radial coordinate of source point
r	Radial coordinate of observation point
ϕ'	Azimuthal coordinate of source point
ϕ	Azimuthal coordinate of observation point
I_1	Integral 1 as defined by the quasi-static aperture admittance model
I_2	Integral 2 as defined by the quasi-static aperture admittance model
φ_{ck}	Volume fraction of the k^{th} inclusion
φ	Cell volume fraction
n	Depolarization factor
ε^*_{debye}	Complex permittivity as per the Debye function (relative)
Γ_T	True reflection coefficient
Γ_m	Measured reflection coefficient
Γ_w	Water Reflection coefficient

$\Gamma_{mi \text{ for } i = 1,2,3.}$	Measured reflection coefficient of calibration standard *i*
$S_{ij \text{ for } i \& j = 1, 2.}$	Scattering parameter of 2-port network
Y_w	Admittance of water
$\bar{x}$	Measured parameter
x	Theoretical parameter
E_n	Normalized error
N_{cells}	Cell number
ϕ_{meas}	Cell volume fraction
N_{cal}	Cell number used for calibration
ϕ_{cal}	Cell volume fraction used for calibration
r^2	Correlation coefficient squared
VAF	Variance accounted for: r^2
CP	Complex permittivity
CPM	Complex permittivity measurement
ECM	Extra-cellular matrix
EMA	Effective medium approximation
α-MEM	Alpha minimum essential medium
PBS	Phosphate buffered solution
EM	Electromagnetic
TEM	Transverse electromagnetic
TE	Transverse electric
TM	Transverse magnetic

The paradigm of tissue engineering is to harvest cells from a patient, expand them in culture, seed them onto a three dimensional scaffold, and cultivate the cell-scaffold construct until the resulting tissue is ready for implantation back into the patient [1-3], as depicted in Fig. 1.1. Current research is expanding on the tissue engineering paradigm by focusing on the application of embryonic stem cells as a cell source for the regeneration of any tissue *in vitro* [4,5]. The increasing average age of the western population has been paralleled with greater incidences of osteoporosis, diabetes, cardiovascular disease, Alzheimer's, and Parkinson's diseases [2]. Tissue engineering promises a more permanent solution to the treatment of damaged and diseased tissues than current surgical and pharmaceutical methods [6].

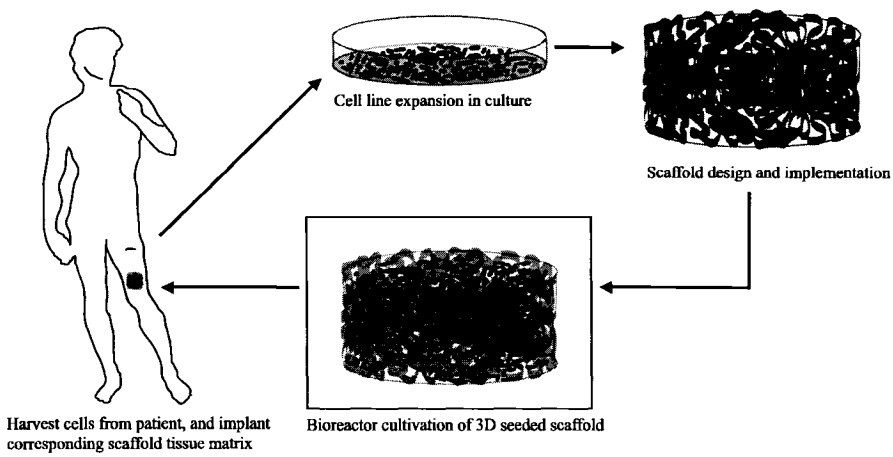

Figure 1.1. Tissue engineering paradigm

Scaffold design and implementation plays an integral role in tissue engineering. Generally, the role of the scaffold is to provide provisional spatial support to guide the complex multicellular processes of tissue formation [7]. Although various materials have been explored for scaffold design, polymers have been used most [8]. Polymer scaffolds have been used as cell-polymer constructs for: vascular grafts, liver equivalents, intestinal tubes, cartilage, and cell carriers

for implantation [9]. Micro-porous polymer scaffolds are a popular choice for tissue engineering applications due to their malleability which permits them to be formed into three-dimensional solid shapes, high porosity which allows nutrient diffusion, and a surface chemistry that permits cell adhesion, proliferation, and differentiation [10].

Tissue growth within scaffolds can be further manipulated by the application of growth factors – cytokines that are secreted by cells and function as signaling molecules. Growth factors can prevent or promote cell adhesion, proliferation, and differentiation. The successful application of growth factors has been hampered by the challenge of identifying their optimal mix and dosage [11].

Ideally, one would record cell proliferation and differentiation to monitor the stages of tissue development and modify the cultivation environment correspondingly. However, current methods of monitoring constituent variation within scaffolds are laborious, often inaccurate, and compromise the sample's integrity [12]. Nuclear magnetic resonance offers a direct measure of cell growth but is a complex procedure that is extremely costly [13]. Capacitance measurements of cell suspensions and immobilized cells have produced good measures of cell concentration but the method cannot be used for three-dimensional scaffolds of, potentially, haphazard shape [14]. The most popular methods of measuring cell proliferation are indirect assays modified from their application to two-dimensional monolayer cultures of low cell densities. Such assays usually measure the metabolic activity or quantify DNA or its pre-cursors. Generally, these cell proliferation assays are destructive and do not necessarily correlate linearly with cell densities [12]. In fact, none of these methods are suitable for the on-line measurement of cell growth within three-dimensional micro-porous scaffolds.

A novel nondestructive method that uses a complex permittivity measurement (CPM), over a frequency range of 100 – 1200 MHz, as a means of monitoring cell differentiation and proliferation on-line in the relevant scaffold was proposed recently by Bagnaninchi *et al* [15-17]. Complex permittivity (CP) gives a measure of a material's response to an applied electric field as a function

of frequency. There are numerous methods of measuring CP, however, the most ubiquitous for biological media is the reflective method, also referred to as impedance spectroscopy. Open-ended coaxial probes are used in conjunction with an impedance analyzer to measure the sample impedance. This is then related to the sample's CP by a model of the probe's aperture admittance. Finally, an effective medium approximation (EMA) is used to relate sample constituents to the CPM.

CPM has been implemented as a diagnostic tool for industrial and medical bioprocesses [18-20]. Thus far, the application of CPM to tissue engineering has been largely limited to the measurement of cell concentration within a cell suspension [18,21]. The extension of the method to monitor tissue growth within polymer scaffolds permitted the non-invasive evaluation of the inner-happenings of the cell-polymer construct. Indeed, the CPM method was successful in determining the porosity of the scaffold, discriminating between different cell-lines, observing stem cell differentiation, and recording the change in cell concentration during the pre-tissue stage of incubation [15-17]. However, prolonged CPM monitoring of the cell-polymer construct revealed that the presence of significant cell side-product formation in the scaffold, particularly the extra-cellular matrix (ECM), causes the cell concentration to be underestimated [17]. Furthermore, for frequencies below 200 MHz, where CPM is most sensitive to cell concentration variation, the real part of CPM was corrupted by polarization effects, limiting the system to higher frequency operation.

The focus of this thesis is to present a comprehensive methodology for the highly responsive measurement of cell constituents based on the CP of a seeded scaffold over a frequency range of 10 – 200 MHz. A novel re-formulation of the EMA is used to eliminate the system's dependence on the real part of the measurement, allowing for low frequency operation. The theory and application of the system elements as tailored for the tissue engineering application are presented.

The system functionality and performance is evaluated from CPMs made from scaffolds with incrementally greater cell concentrations. Results showed that the system can distinguish between scaffolds of different cell concentration.

Last, the system was used to monitor cell proliferation within scaffolds over a period of two weeks. In conjunction, a DNA assay was used to produce a proliferation curve for comparison and validation. Scanning electron microscopy (SEM) analysis was also performed to identify cell presence, morphology, and scaffold structure. The results showed that the system measures the relative change of pre-osteoblast cell concentration in the scaffolds in a manner comparable to a DNA assay.

1.1 Thesis Hypothesis

The sensitivity of the cell concentration measurement within a polymer scaffold by way of a complex permittivity measurement (CPM) will increase at lower frequencies (10 – 200 MHz). In addition, the cell concentration measurement can be made using only the imaginary part of this CPM.

1.2 Thesis Objectives

The primary objective of this thesis was to develop and validate a thorough methodology for the measure of cell constituent variation within a three-dimensional micro-porous scaffold at frequencies of 10 - 200 MHz. To achieve this primary goal the following specific objectives have to be reached:

1. To propose the appropriate instrumentation for CPM, i.e., the desired open-ended probe dimensions, and appropriate material analyzer.
2. To propose and implement an optimal procedure for the CPM of scaffolds.
3. To propose, implement, and test an appropriate model of the probe's aperture admittance for the current tissue engineering application.

4. To propose, implement, and test a method for the removal of the real part of the CPM at low frequencies.
5. To demonstrate the capability of the system to discriminate between scaffolds seeded with different cell concentrations.
6. To produce a standard cell proliferation curve via an online daily CPM of cell seeded scaffolds over a period of 14 days.

1.3 Thesis Outline

This thesis is comprised of the current introductory chapter, a literature review (chapters 2-5), a manuscript (chapter 6), and a general conclusion (chapter 7) followed by three appendices. A brief description of chapter contents is presented below:

- Chapter 1 presents a summary of the proposed application context, necessity, and function. The chapter also includes the thesis hypothesis, objectives and provides the reader with the thesis outline.
- Chapter 2 is an overview of the use of three-dimensional cultures in tissue engineering and methods for cell proliferation measurement.
- Chapter 3 presents the reader with an overview of dielectric theory necessary for the application.
- Chapter 4 discusses the different methods of permittivity measurement and presents the open-ended coax as the permittivity probe along with the appropriate corresponding aperture admittance models.
- Chapter 5 concludes the literature review with a discussion of how cell concentration measurements are performed via permittivity. The chapter focuses on effective medium theory and its application to cell concentration measurement for cell suspensions and scaffolds.
- Chapter 6 is comprised of a manuscript that will be submitted to an appropriate journal: "A System for the On-line *in-vitro* Monitoring of Tissue Development within Micro-Porous Polymer Scaffolds". This

manuscript contains a concise introduction and theoretical background of the topic, as well as, the methodology and experiments used to fulfill objectives 1-6. The results, discussion, and conclusion sections of the manuscript present the appropriate analysis and performance evaluation of the system.

- Chapter 7 provides a summary and general conclusion of the work, as well as possible perspectives for future work and applications of the proposed system.
- Appendix A of the thesis contains an accepted proceedings paper for the IEEE Engineering in Medicine and Biology Society: "A Highly Responsive System for On-line *in vitro* Assessment of Tissue Growth within Micro-Porous Polymer Scaffolds".
- Appendix B presents the MatLab programming code that was applied to implement the analytical stages of the system.
- Appendix C comprises the form necessary to use biohazardous materials for experiments.

1.4 References

[1] J. J. Marler, J. Upton , R. Langer , and J. P. Vacanti, "Transplantation of Cells in Matrices for Tissue Regeneration," Advanced Drug Delivery Reviews, vol. 33, pp. 165-182, 1998.

[2] S. Petit-Zeman, "Regenerative Medicine," Nature Biotechnology, vol. 19, pp. 201-206, 2001.

[3] L. G. Griffith, and G. Naughton, "Tissue Engineering-Current Challenges and Expanding Opportunities," Science, vol. 295, pp. 1009-1016, 2002.

[4] R. P Lanza, H. Y. Chung, J. J. Yoo, P. J. Wettstein, C. Blackwell, N. Borson, E. Hoffmeister, G. Schuch, S. Soker, C. T. Moraes, M. D. West, and A. Atala, "Generation of Histocompatible Tissues using Nuclear Transplantation," Nature Biotechnology, vol. 20, pp. 689-696, 2002.

[5] S. Battista, D. Guarnieri, C. Borselli, S. Zeppetelli, A. Borzacchiello, L. Mayol, D. Gerbasio, D. R. Keene, L. Ambrosio, and P. A. Netti, "The

Effect of Matrix Composition of 3D Constructs on Embryonic, Stem Cell Differentiation," Biomaterials, vol. 26 pp. 6194-6207, 2005.

[6] "Tissue Engineering," Nature Biotechnology, vol. 18, supplement, pp. 56-58, 2000.

[7] P. X. Ma, "Scaffolds for Tissue Fabrication," Materials Today, Review Feature, pp. 30 - 40, 2004.

[8] R. Langer, and D. A. Tirrell, "Designing Material for Biology and Medicine" Nature Review, vol. 428, pp. 487-492, 2004.

[9] L. E. Freed, G. Vunjak-Novakovic, R. J. Biron, D. B. Eagles, D. C. Lesnoy, S. K. Barlow, and R. Langer, "Biodegradable Polymer Scaffolds for Tissue Engineering," Nature Biotechnology, vol. 12, pp. 689-693, 1994.

[10] D. W. Hutmacher, "Scaffolds in Tissue Engineering Bone and Cartilage," Biomaterials, vol. 21, pp. 2529-2543, 2000.

[11] F. R. A. J. Rose, and R. O. C. Oreffo, "Bone Tissue Engineering: Hope vs Hype," Biochemical and Biophysical Research Communications, vol. 292, pp. 1–7, 2002.

[12] W. Ng, D. T. Leong, and D. W. Hutmacher, "The Challenge to Measure Cell Proliferation in Two and Three Dimensions," Tissue Engineering, vol. 11(1-2), pp. 182-191, 2005.

[13] G. Locher, B. Sonnleitner, and A. Fiechter, "On-line Measurement in Biotechnology: Techniques," Journal of Biotechnology, vol. 25, pp. 23–53, 1992.

[14] P. Ducommun, A. Kadouri, U. von Stockar, and I. W. Marison, "On-line Monitoring of Animal Cell Concentration in Two Industrial High-Density Culture Processes by Dielectric Spectroscopy," Biotechnology and Bioengineering, vol. 77, pp. 316–317, 2002.

[15] P. O. Bagnaninchi, M. Dikeakos, T. Veres, and M. Tabrizian, "Monitoring of Stem Cell Proliferation and Differentiation using a Permittivity Responsive Biointerface", Materials Research Society Symposium Proceedings, vol. 773, pp. N7.12.1, 2003.

[16] P. O. Bagnaninchi, M. Dikeakos, T. Veres, and M. Tabrizian, "Towards On-line Monitoring of Cell Growth in Microporous Scaffolds: Utilization and Interpretation of Complex Permittivity Measurements" Biotechnology and Bioengineering, vol. 84, pp. 343-350, 2003.

[17] P. O. Bagnaninchi, M. Dikeakos, T. Veres, and M. Tabrizian, "Complex Permittivity Measurement as a New Non-invasive Tool for Monitoring In-vitro Tissue Engineering and Cell Signature Through the Detection of Cell Proliferation, Differentiation, and Pre-tissue Formation," IEEE Transactions on Nanobioscience, vol. 3, pp. 243-250, 2004.

[18] K. Asami, "Characterization of Biological Cells by Dielectric Spectroscopy," Journal of Non-Crystalline Solids, vol. 305(1-3), pp. 268-277, 2002.

[19] R. Pethig, and D. B. Kell, "The Passive Electrical Properties of Biological Systems: Their Significance in Physiology, Biophysics and Biotechnology," Physics in Medicine and Biology, vol. 32, no. 8, pp. 933-970, 1987.

[20] J. P. Grant, R. N. Clarke, G. T. Symm, and N. M. Spyrou, "A Critical Study of the Open-Ended Coaxial Line Sensor Technique for RF and Microwave Complex Permittivity Measurements," Journal of Physics E: Scientific Instruments, vol. 22, pp. 757-770, 1989.

[21] G. H. Markx, and C. L. Davey, " The Dielectric Properties of Biological Cells at Radiofrequencies: Applications in Biotechnology," Enzyme and Microbial Technology, vol.25(3-5), pp.161-171, 1999.

CHAPTER 2

Three-Dimensional Scaffolds

The three-dimensional (3D) scaffold is the basis for *in vitro* simulation of the *in vivo* environment necessary for successful tissue engineering. A lot of interest has been directed to the exploration of 3D cell culture [1-3]. Consequently, the differences between 2D and 3D culture are becoming known [1]. The operative difference between 2D and 3D culture techniques is the presence of extra-cellular matrix (ECM) in 3D cell growth. In mammalian culture, cells not only attach to each other but also to the support structure that is the ECM. The ECM is formed of proteins such as elastin, laminin, and collagen that give tissue its specific mechanical properties and help cells communicate between each other. The communication mechanism comprises proteins, such as Integrins, on the cell surface that attach themselves to the ECM and modulate the biochemical cues from their immediate environment. Studying cells only in flat layers eliminates these subtle mechanics [2]. Thus, cells behave differently in 3D than in 2D cultures. The importance of this difference was demonstrated in a landmark paper [4] that reported that antibodies against a surface receptor changed the behavior of cancerous breast cells grown in 3D culture to seemingly non-cancerous cells – a phenomenon that was not observed in 2D culture. Another noted difference between 3D and 2D culture is that the gene expression profile in 3D is much closer to that *in vivo*. In general, it is now acknowledged that an *in vivo* environment is better mimicked by a 3D scaffold. Consequently, the application of 3D scaffolds has been the focus of research in cancer [4], developmental biology [3], and especially tissue engineering [5].

Tissue engineering applications generally require the following scaffold characteristics: i) high porosity to facilitate nutrient diffusion, ii) enough mechanical strength to support the growth of tissue, iii) malleability to allow the construction of the necessary 3D support architecture, iv) surface chemistry that permits cell attachment, proliferation, and differentiation, v) biocompatibility, to prevent undesired immune reactions in the patient [6-9].

As the paradigm of medicine shifts from using synthetic implants to the tissue engineering approach, the demand for scaffold technology is increasing. There are various types of material matrices used to form scaffolds. To successfully grow cells in 3D, cells must be embedded in a matrix that resembles the ECM. There are two types of 3D scaffolds: gels and solid-state.

2.1 Gel Matrices

Gels have been a popular choice for cell culture and cell observation in a 3D construct. Commercial gels such as Matrigel are concoctions of substances derived from a type of mouse tumor and have been much used over the past 20 years [1]. Other types of gels, that retain cell viability, have been used as immobilizing constructs and as cell transport vehicles. Hydrogel-based materials have been popular in biomedical applications as vehicles for drug, or bioactive molecule, delivery [10]. The challenge with hydrogel application is to maintain cell viability throughout the gel preparation process. In most procedures, to embed cells into a gel, pre-gel solutions are mixed with the cells and gellation is induced via chemical or physical cross-linking. It is also a challenge to create uniform gels because the structure is highly dependent on the induced gellation rate [11]. Cells seeded in a gel are not attached to any structure but are suspended by the viscosity of the embedding matrix. As a result, hydrogels are not often used as supports for tissue formation because they lack the mechanical structure required for tissue regeneration. However, the architecture is conducive for injectable delivery of the cell-gel construct.

2.2 Solid State Scaffolds

Solid state scaffolds generally do not dissolve or melt in *in vitro* or *in vivo* conditions and so must be implanted into the patient. The most common materials used for these scaffolds are linear aliphatic polyesters. There are numerous such polymers that distinguish themselves by their degradation properties. Natural

polymers such as proteins and polysaccharides are also used for tissue engineering applications.

Collagen has been used often, especially for soft tissue repair, because it is a natural component of the ECM. However, collagen applications are susceptible to pathogen transfer and consequent immune reactions [12]. In addition, the collagen biodegradation rates are difficult to control and the mechanical properties are poor [12].

Recently, silk has been explored as a potential material for scaffolds. Silk has previously been used for sutures and has excellent mechanical properties [13, 14]. Silk is generally considered to be non-degradable; however, it has been shown to slowly degrade *in vivo* due to enzymatic function which raises concerns about its cytotoxicity [10].

Another natural polymer that has received a lot of attention is chitosan [15]. Chitosan is a polysaccharide, a partially deacetylated derivative of chitin which forms the primary structural polymer in arthropod exoskeletons. Chitosan is biodegradable and has previously been used for wound dressings [16], drug delivery systems [17], and space filling implants [18]. Although the application of chitosan to tissue engineering is relatively novel, chitosan micro-porous scaffolds have been characterized for various architectures [19]. Chitosan was the polymer chosen for the scaffolds used in this thesis because it well represents the current trend in biomaterials, the chitosan micro-porous scaffold adheres well to the probe's surface, and it supports Osteoblast and Chondrocyte survival and phenotypic expression [19].

There have been a number of inorganic materials used for scaffold construction, usually for bone tissue engineering [10]. Some metals have been used because they support osteoblastic cell adhesion, growth and differentiation; as well, they promote bone tissue formation [20, 21]. The drawback of these materials is that they are brittle and difficult to manipulate into a highly porous scaffold.

Composite materials have been developed to optimize the performance of the scaffold [22,23]. These materials have been used to produce highly porous

scaffolds which are strong enough mechanically to sustain bone tissue formation [23].

2.3 Measuring Cell Proliferation in 3D Scaffolds

In the past decade there has been a 20 % increase in the number of publications related to cell culture proliferation assays [24]. The cell proliferation parameter is specifically of great interest in tissue engineering as a measure of tissue growth. Current assays used for 3D cultures are adaptations of 2D culture assays [24]. Proliferation assays either measure metabolic activity [25], DNA [26], a radioactive label [27], or the cells are manually counted by a hemacytometer. Not all the assays are destructive, i.e., in certain cases the cells do not have to be lysed prior to counting. However, it is important to underline that all the assays require the isolation of the cells from the scaffold – each assay has its particular protocol – and so are not on-line measurements. In addition, only manual cell counting can quantify cell numbers, the other methods are approximates or relative measurements.

Hutmacher *et al* [24] conducted a study that assessed the performance of proliferation measurement techniques in 3D scaffolds; they reported that the assay results do not necessarily correlate linearly with increasing cell density. In general, they suggested that cell proliferation assays in 3D cultures should be used with caution and only as a rough approximation of cell growth.

2.4 Chapter Segue

This chapter underlined the significance of 3D cell culture and elaborated on the application of scaffolds in tissue engineering. Different kinds of scaffolds were introduced to give the reader a breadth of how robust and significant scaffold design is. Chitosan was introduced as a polymer often used for biomedical applications and the polymer that is used here for the micro-porous

polymer scaffolds. The chapter concluded with a description of the shortcomings of current assay methods for measuring cell proliferation in 3D scaffolds.

The next chapter introduces the reader to the permittivity theory necessary to understand the function of the new system. It is appropriate to underline here that the new system can perform a cell concentration measurement without any compromise to sample integrity. Consequently, the cell concentration in a specific scaffold can be measured throughout a cultivation period resulting in a proliferation curve – this is impossible with current cell proliferation assays. Furthermore, the system's cell concentration measurement requires a minimal preparation protocol when compared to cell proliferation assays.

2.5 References

[1] A. Abbot, "Biology's New Dimension," Nature, vol. 424, pp. 870-872, 2003.

[2] S. Kale, S. Biermann, C. Edwards, C. Tarnowski, M. Morris, and M. W. Long, "Three Dimensional Cellular Development is Essential for *Ex-vivo* Formation of Human Bone," Nature Biotechnology, vol. 18, pp. 954-958, 2000.

[3] E. Cukierman, R. Pankov, D. R. Stevens, and K. M. Yamada, "Taking Cell Matrix Adhesions to the Third Dimension," Science, vol. 294, pp. 1708-1712, 2001.

[4] V. M. Weaver, O. W. Petersen, F. Wang, C. A. Larabell, P. Briand, C. Damsky and M. J. Bissell, "Reversion of the Malignant Phenotype of Human Breast Cells in Three-Dimensional Culture and *In vivo* using Integrin Blocking Antibodies," Journal of Cell Biology, vol. 137, pp. 231-246, 1997.

[5] S. J. Hollister, "Porous Scaffold Design for Tissue Engineering," Nature Materials, vol. 4, pp. 518-524, 2005.

[6] D. W. Hutmacher, "Scaffolds in Tissue Engineering Bone and Cartilage," Biomaterials, vol. 21, pp. 2529-2543, 2000.

[7] L. Meinel, V. Karageorgiou, R. Fajardo, B. Snyder , V. Shinde-Patil, L. Zichner, D. Kaplan, R. Langer, and G. Vunjak-Novakovic, "Bone Tissue Engineering using Human Mesenchymal Stem Cells: Effects of Scaffold

Material and Medium Flow," Annals of Biomedical Engineering, vol. 32, pp. 112-122, 2004.

[8] V. Karageorgiou, and D. Kaplan, "Porosity of 3D Biomaterial Scaffolds and Osteogenesis," Biomaterials, vol. 26, pp. 5474-5491, 2005.

[9] T. B. F. Woodfield, J. Malda, J. De Wijn, F. Peters, J. Riesle, and C. A. Van Blitterswijk, "Design of Porous Scaffolds for Cartilage Tissue Engineering using a Three-Dimensional Fiber-Deposition Technique," Biomaterials, vol. 25, pp. 4149-4161, 2004.

[10] P. X. Ma, "Scaffolds for Tissue Fabrication," Materials Today, review feature, pp. 30-40, 2004.

[11] C. K. Kuo, and P. X. Ma, "Ionically Crosslinked Alginate Hydrogels as Scaffolds for Tissue Engineering: Part 1. Structure, Gelation Rate and Mechanical Properties," Biomaterials, vol. 22, pp. 511-521, 2001.

[12] D. W. Hutmacher, J. C. Goh, S. H. Teoh, "An Introduction to Biodegradable Materials for Tissue Engineering Applications," Annals Academy of Medicine Singapore, vol. 30, pp. 183-191, 2001.

[13] S. Hofmann, D. Kaplan, G. Vunjak-Novakovic, H. P. Merkle1, R. Langer, and L. Meinel, "Engineering Cartilage-Like Tissue from Human Mesenchymal Stem Cells on Silk Scaffolds" European Cells and Materials, vol. 7, pp. 13, 2004.

[14] L. Meinel, V. Karageorgiou, S. Hofmann, R. Fajardo, B. Snyder, C. Li, L. Zichner, R. Langer, G. Vunjak-Novakovic, and D. L. Kaplan, "Engineering Bone-Like Tissue *In-vitro* using Human Bone Marrow Stem Cells and Silk Scaffolds," Journal of Biomedical Materials Research Part A, vol. 71, pp. 25-34, 2004.

[15] S. B. Rao and C. P. Sharma, "Use of Chitosan as a Biomaterial: Studies on its Safety and Hemostatic Potential," Journal of Biomedical Materials Research, vol. 34, pp. 21–28, 1997.

[16] J. M. Yang and H. T. Lin, "Properties of Chitosan Containing PP-g-AA-g-NIPAAm Bigraft Nonwoven Fabric for Wound Dressing," Journal of Membrane Science, vol. 243, pp. 1-7, 2004.

[17] M. M. Issa, M. Köping-Höggård and P. Artursson, "Chitosan and the Mucosal Delivery of Biotechnology Drugs," Drug Discovery Today: Technologies, vol. 2, pp. 1-6, 2005.

[18] E. Khor and L. Yong Lim "Implantable Applications of Chitin and Chitosan," Biomaterials, vol. 24, pp. 2339-2349, 2003.

[19] S. V. Madihally, and H. W. T. Matthew, "Porous Chitosan Scaffolds for Tissue Engineering," Biomaterials, vol. 20, pp. 1133-1142.

[20] J. P. St-Pierre, M. Gauthier, L. P. Lefebvre and M. Tabrizian, "Three-Dimensional Growth of Differentiating MC3T3-E1 Pre-Osteoblasts on Porous Titanium Scaffolds" Biomaterials, In Press, Available July 2005.

[21] E. D. Spoerke, N. G. Murray, H. Li, L. C. Brinson, D. C. Dunand and S. I. Stupp, "A Bioactive Titanium Foam Scaffold for Bone Repair" Acta Biomaterialia, In Press, Available July 2005.

[22] M. Zhang, X. H. Li, Y. D. Gong, N. M. Zhao and X. F. Zhang, "Properties and Biocompatibility of Chitosan Films Modified by Blending with PEG," Biomaterials, vol. 23, pp. 2641-2648, 2002.

[23] R. Zhang, Peter X. Ma, "Poly(a-hydroxyl acids)/Hydroxyapatite Porous Composites for Bone-Tissue Engineering. I. Preparation and Morphology," Journal of Biomedical Materials Research, vol. 44, pp. 446-455, 1998.

[24] K. W. Ng, D. T. Leong, D. W. Hutmacher, "The Challenge to Measure Cell Proliferation in Two and Three Dimensions", Tissue Engineering, vol. 11, pp. 182-191, 2005.

[25] M. M. Nociari, A. Shalev, P. Benias, and C. Russo, "A Novel One-Step, Highly Sensitive Fluorometric Assay to Evaluate Cell Mediated Cytotoxicity,"Journal of Immunological Methods, vol. 213, pp. 157, 1998.

[26] S. J. Ahn, J. Costa and J. R. Emanuel, "PicoGreen Quantitation of DNA: Effective Evaluation of Samples Pre- or Post-PCR," Nucleic Acids Research, vol. 24, pp. 2623, 1996.

[27] L. E. Feinendegen, "Tritium-Labeled Molecules in Biology and Medicine," New York: Academic Press, 1967.

CHAPTER 3
Permittivity

3.1 Permittivity Theory

Permittivity describes how a material, invariant of its quantity, will react to and modify an applied electric field. When an electric field is applied to a medium it elicits electric responses of charge migration and reorientation of electric dipoles that correspond to two types of current flow: conduction and displacement. It is the displacement current, which is the elastic response of a material to an electric field and not a current of electric charge, that is of interest. When the electric field is increased, the current is stored and when the field is decreased the current is released. The electric displacement field is defined by the resulting field in a linear material:

$$\vec{D} = \varepsilon\vec{E} \quad \left(C/m^2\right), \tag{3.1}$$

Where ϵ is the absolute permittivity, $\vec{E}$ is the electric field, and $\vec{D}$ is the electric displacement field. The displacement current is the time derivative of $\vec{D}$.

From (3.1) it is evident that knowing $\vec{E}$ and measuring $\vec{D}$ would reveal the permittivity of the medium. The electric displacement field can also be expressed as:

$$\vec{D} = \varepsilon_0\vec{E} + \vec{P} \quad \left(C/m^2\right), \tag{3.2}$$

where ϵ_0 is the permittivity of vacuum (8.854 pF m^{-1}) and $\vec{P}$ is the polarization of the material.

Consequently it is the polarization that describes the electric displacement field within the material:

$$\vec{P} = (\varepsilon_r - 1)\varepsilon_0\vec{E} \quad \left(C/m^2\right), \tag{3.3}$$

where $\varepsilon_r = \varepsilon/\varepsilon_0$, is the relative permittivity. Relative permittivity is a unit-less measure of the polarizability of a material. From this point forward, unless specified to be absolute, the term permittivity will be used to mean relative permittivity and the subscript *r* will be dropped for convenience.

Dielectric polarization is a measure of the material's capability of neutralizing the applied electric field. There are four types of dielectric polarizations, and their combinations, that can occur: electronic, ionic, orientational, and interfacial.

- Electronic polarization refers to the displacement of the electron cloud relative to the nucleus in response to an applied electric field, as shown in Fig. 3.1A.
- Ionic polarization refers to the displacement of a molecule's ions in response to an applied electric field, as shown in Fig. 3.1B.
- Orientational polarization refers to the reorientation of the material's dipoles toward the applied electric field vector as shown in Fig. 3.1C.
- Interfacial polarization refers to the accumulation of mobile charge carriers at an interface in response to an applied electric field as shown in Fig. 3.1D.

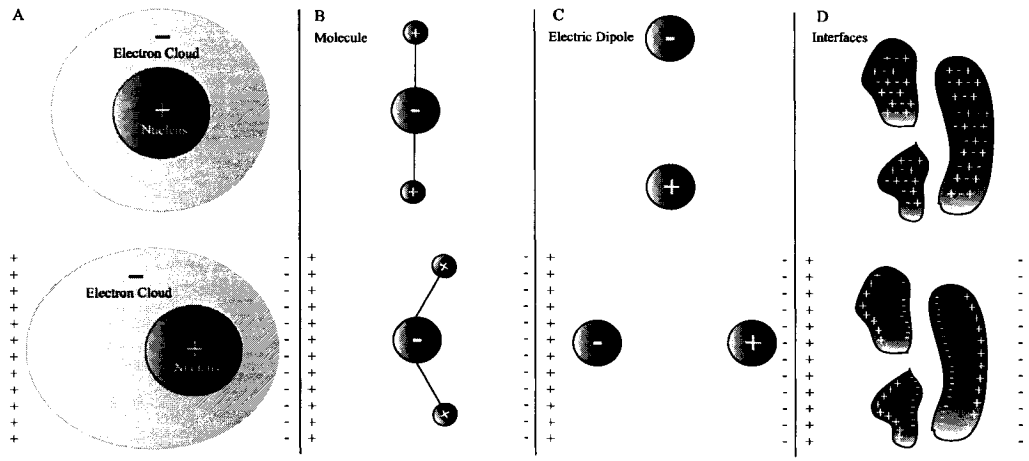

Figure 3.1. The different polarization mechanisms: A) atomic polarization, B) molecular polarization, C) orientational polarization, D) interfacial polarization

Electronic and ionic polarization mechanisms are only significant at optical and far-infrared electric field frequencies (> 10^{11} Hz) respectively and therefore will not be discussed further. Interfacial and orientational mechanisms are based on larger masses and so respond more slowly to the application and

removal of an electric field; therefore, they are primarily prevalent at lower frequencies (< 10^{11} Hz).

3.1.1 Complex Permittivity

A material's response to an applied electric field is causal because of the delayed interfacial and orientational polarizations. Consequently, permittivity is a complex function of applied electric field frequency:

$$\varepsilon^*(\omega) = \varepsilon'(\omega) - j\varepsilon''(\omega), \tag{3.4}$$

where $j = \sqrt{-1}$, ε' is the real permittivity , ε'' is the imaginary permittivity also known as the loss factor, and ω is the angular frequency of the applied excitation electric field.

In the ideal case, when a static electric field is applied to a material it gives rise to a volume density polarization in the direction of the field, the permittivity is then referred to as static and is purely real. At very low frequencies the induced polarization vector will be synchronized with the applied alternating electric field vector. As the frequency of the field increases the inertia of the charged particles retard the polarization vector and cause it to become out of phase with the field as depicted by Fig. 3.2.

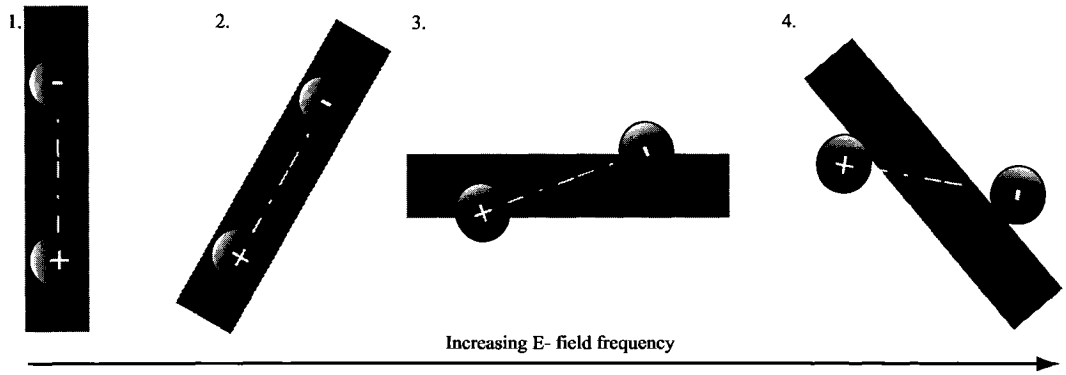

Figure 3.2. Progressively developing phase lag between applied electric field and a dipole

The retardation and relaxation processes are characterized by energy loss due to frictional damping mechanisms. Furthermore, if the affected material has a

significant number of free charge carriers, such as ions in an electrolyte solution, ohmic losses will ensue. Both types of losses are accounted by the loss factor:

$$\varepsilon'' = \frac{\sigma_S + \sigma_D}{\varepsilon_0 \omega} = \frac{\sigma}{\varepsilon_0 \omega} \tag{3.5}$$

where σ_S and σ_D are, respectively, the static (ionic) and dynamic (orientational) conductivity and σ is the total conductivity. It is important to underline here, that for ionic solutions, such as saline and biological media the static conductivity is much larger than the dynamic conductivity. The loss factor is always greater than zero. At optical frequencies permittivity reaches a constant sometimes referred to as the optic permittivity (ε_∞).

The real permittivity, sometimes termed the dielectric constant, relates the amount of energy stored per unit volume in the material to the applied electric field. For the majority of solids and liquids $\varepsilon'(\omega) > 1$.

The phase of complex permittivity is referred to as the loss angle as graphically depicted in Fig. 3.3. The *tan* of the loss angle is referred to as the loss tangent because it is related to the amount of power loss in the medium:

$$\tan\partial = \frac{\varepsilon''}{\varepsilon'} \cong \frac{\sigma}{\omega\varepsilon}. \tag{3.6}$$

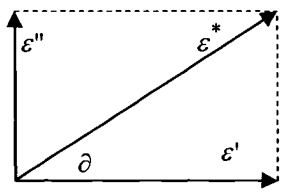

Figure 3.3. Graphical depiction of complex permittivity

As the frequency of the applied electric field increases toward microwave frequencies the effects of the interfacial and orientational polarizations decline. As a result, the real permittivity decreases and the loss tangent increases.

3.1.2 Dipole Relaxation

The relaxation of dipoles excited by an applied electric field decays approximately exponentially. Assuming no interaction between dipoles, the

relaxation has been modeled by a first order equation known as the Debye equation [1]:

$$\varepsilon^*(\omega) = \varepsilon_\infty + \frac{\varepsilon_s - \varepsilon_\infty}{1 + j\omega\tau}, \tag{3.7}$$

where τ is the characteristic time constant, ε_s and ε_∞ are the static and optic permittivities. The values of $\varepsilon_s, \varepsilon_\infty$, and τ have been experimentally determined for various standard media over years of research [2-4]. Other more robust models have been proposed, applied, and summarized by Assami in [5]. Numerous dispersions of heterogeneous media such as biological tissue have been successfully described as the sums of these formulations [5].

3.1.3 Electrode Polarization Effects

The measurement of permittivity in conductive materials by way of electrodes is often corrupted by a parasitic phenomenon known as electrode polarization [6]. Electrode polarization is the accumulation of charge at the sample-electrode interface and the formation of an electrical double layer [7], as depicted in Fig. 3.4. The electrical double layer misrepresents the constitution of the sample under measurement. Specifically, the permittivity spectrum of the sample becomes corrupt at frequencies, usually below 100 MHz [7, 8]. The effect of the electrical double layer is a function of the surface topography, chemistry, and area of the electrode as well as the chemistry of the sample. Since the extent of the phenomenon is very case specific there is no widely accepted correction technique. The most prevalent techniques in modeling electrode polarization are presented in [7, 9, 10].

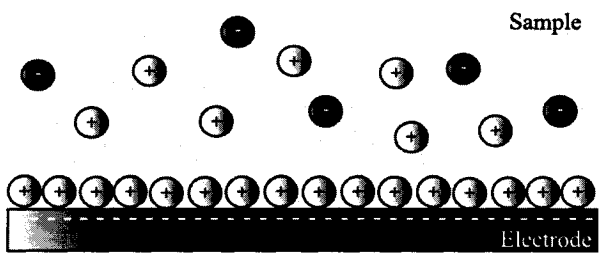

Figure 3.4. Electrode polarization: rendition of an electrode immersed in an electrolyte

3.1.4 Temperature Effects

Complex permittivity is a function of temperature. Using saline as the relevant heuristic example, at higher temperatures the strength and extent of molecular bonds tend to decrease. Consequently, the static and optical permittivity is lowered; ions can react to the alternating potential at lower frequencies; the dipole is freer to oscillate at higher frequencies; the drag to the rotating molecules is reduced. Research on the temperature dependence of the complex permittivity of mammalian tissue, specifically on blood [11], liver [12], and skin [13] has been done. A specific tissue generally contains highly ionic fluids so many observations can be explained by the complex permittivity behavior of saline. The results of these biological measurements, of relevance to this work, are that the interfacial polarization of cells shifts towards lower frequencies with increasing temperature.

3.2 Complex Permittivity of Biological Tissue

Complex permittivity spectroscopy of biological tissue has been used since the beginning of last century [14-17]. These early permittivity studies showed that erythrocytes are composed of a poorly conducting membrane enclosing an electrolyte. H. P. Schwan [18-21] pioneered biological tissue characterization through permittivity by formulating the foundations for modeling the dispersion of a biological cell suspension in an electrolyte. Subsequently, advances in technology and medicine have led to a plethora of research in the application of permittivity for biological tissue characterization.

The complex permittivity spectra of biological tissues have a common behavior depicted by Fig. 3.5. The real permittivity will be highest at low frequencies and will decrease in progressively distinct steps with the excitation frequency. The median value between two levels corresponds to the characteristic frequency. The loss factor remains low and then peaks at the characteristic

frequencies of the different dispersions. The term dispersion, as applied here, refers to a transition between the upper and lower plateaus of the distinct steps of real permittivity. The four major dispersions found in a complex permittivity spectrum of biological tissue are depicted in Fig. 3.5. The α-dispersion, although not well understood, has been correlated with the cellular membrane potential [22], sarcoplasmic reticulum [23], gap junctions [24], and the displacement of counter ions surrounding charged membranes [25]. The β-dispersion is due to interfacial polarization across the plasma membrane surrounding the cells, and is central to this thesis. The δ-dispersion is related to biopolymers [25], proteins [24], protein-bound water [24], and cell organelles [25]. The γ-dispersion is due to the polarization of water.

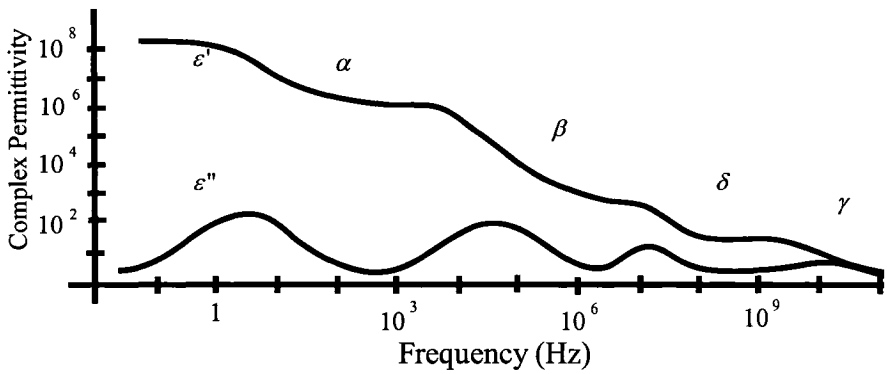

Figure 3.5. Idealized dispersion regions for biological tissue (The DC conductance contribution has been subtracted from the loss factor) [24]

3.2.1 Interfacial Relaxation

The Maxwell-Wagner effect is a process that describes the β-dispersion. A relevant example is to consider a biological cell modeled as a homogenous cytoplasm surrounded by a low-conducting plasma membrane. When immersed in an electrolyte, under equilibrium conditions, the cell will be surrounded by ions of opposite charge forming an electrical double layer as depicted by Fig. 3.6A. An applied electric field will distort the surrounding charge distribution. In effect, an electrical dipole is formed of significant magnitude, relative to molecular dipoles, due to the much greater distance between the opposing charges as depicted by Fig. 3.6B. When an alternating electric field is applied, the dipole does not appear

instantaneously but rather at an exponential rate, similarly to the molecular dipole, with a time constant defined as:

$$\tau = \frac{\varepsilon_{cyt} + 2\varepsilon_m}{\sigma_{cyt} + 2\sigma_m} \quad (s), \tag{3.8}$$

where ε_{cyt} and σ_{cyt} are, respectively, the real absolute permittivity and conductivity of the cytoplasm while ε_m and σ_m are respectively, the permittivity and conductivity of the suspending medium. If $\sigma_{cyt}\varepsilon_m = \sigma_m\varepsilon_{cyt}$ the interface has no free charge density, otherwise the interface is charged. For an electric dipole to occur the cytoplasm permittivity must be different from that of the surrounding medium.

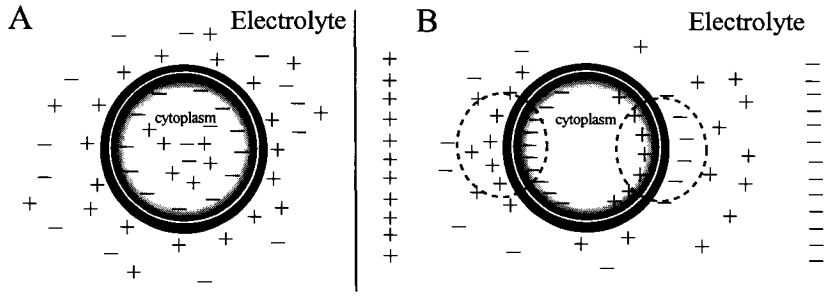

Figure 3.6. Maxwell-Wagner effect: A) Transverse cell model immersed in electrolyte, B) An electric field applied to A) forming a dipole highlighted by the dashed lines.

J. C. Maxwell extended the cell model to include the effects of the plasma membrane enveloping the cytoplasm. The plasma membrane is a lipid bilayer of low ionic permeability and can therefore be considered to be a low conducting thin shell [5]. Note, the cytoplasm is a heterogenous material that contains organelles immersed in cytosol that experience their own polarization effects. In addition, DNA and various proteins will produce their own relaxations. However, the plasma membrane relaxation dominates so the model assumes the cytoplasm to be uniform. The corresponding expression for the permittivity of the single shell cell model is:

$$\varepsilon^*_{cell}(\omega) = \varepsilon^*_{mem}(\omega)\frac{2\varepsilon^*_{mem}(\omega) + \varepsilon^*_{cyt}(\omega) - 2v(\varepsilon^*_{mem}(\omega) - \varepsilon^*_{cyt}(\omega))}{2\varepsilon^*_{mem}(\omega) + \varepsilon^*_{cyt}(\omega) + v(\varepsilon^*_{mem}(\omega) - \varepsilon^*_{cyt}(\omega))}, \tag{3.9}$$

where $v = (1 - d/r_c)^3$, r_c is the outer radius of the cell, d is the thickness of the membrane, ε^*_{mem}, and ε^*_{cell} are, respectively, the complex permittivity of the cell membrane and the cell.

J. C. Maxwell then proposed an expression for the effective permittivity of a suspension of these cell models':

$$\varepsilon^*_{eff}(\omega) = \varepsilon^*_m(\omega)\frac{2\varepsilon^*_m(\omega) + \varepsilon^*_{cell}(\omega) - 2\varphi(\varepsilon^*_m(\omega) - \varepsilon^*_{cell}(\omega))}{2\varepsilon^*_m(\omega) + \varepsilon^*_{cell}(\omega) + \varphi(\varepsilon^*_m(\omega) - \varepsilon^*_{cell}(\omega))}, \tag{3.10}$$

where φ is the cell volume fraction, ε^*_m, and ε^*_{eff} are, respectively, the complex permittivity of the ambient and effective medium.

Equation (3.10) is an effective medium approximation (EMA) for an approximate cell suspension. Chapter 5 will discuss EMA in more detail.

3.3 Chapter Segue

This chapter introduced the permittivity theory that forms the basis behind the function of the system developed in this thesis. Complex permittivity was defined and its dependence on interfacial polarization was discussed. Complex permittivity of biological media was given special attention to introduce the reader to the β-dispersion based on the Maxwell-Wagner effect which is central to this thesis. It was shown that the β-dispersion contains information about the constituents of the biological sample.

The following chapter introduces the methods and materials required for measuring complex permittivity of micro-porous scaffolds in the β-dispersion range.

3.4 References

[1] P. J. W. Debye, "Polar Molecules," New York: Dover Publications, 1929.

[2] M. Razaz and J. B. Davies, "Capacitance of the Abrupt Transition from Coaxial to Circular Waveguide," IEEE Transactions on Microwave Theory Technology, vol. MTT-27, pp. 564-569, 1979.

[3] J. Dibeneditto and A. Uhlir, Jr., "Frequency Dependence of 50-Ω Coaxial Open-Circuit Reflection Standard," IEEE Transactions on Instrumentation and Measurement, vol. IM-30, pp. 228-229, 1981.

[4] H. E. Bussey, "Dielectric Measurements in a Shielded Open Circuit Coaxial Line," IEEE Transactions on Instrumentation and Measurement, vol. IM-29, pp. 120-124, 1980.

[5] K. Asami, "Characterization of Heterogeneous Systems by Dielectric Spectroscopy," Progress in Polymer Science, vol. 27 pp. 1617-1659, 2002.

[6] C. L. Davey, and D. B. Kell, "The Influence of Electrode Polarization on Dielectric Spectra, with Special Reference to Capacitive Biomass Measurements I. Quantifying the Effects on Electrode Polarization of Factors Likely to Occur During Fermentations," Bioelectrochemistry and Bioenergetics, vol. 46, pp. 91-103, 1998.

[7] Y. Feldman, E. Polygalov, I. Ermolina, Y. Polevaya. and B. Tsentsiper, "Electrode Polarization Correction in Time Domain Dielectric Spectroscopy," Measurement Science and Technology, vol. 12, pp. 1355-1364, 2001.

[8] F. Bordi, C. Cametti, and T. Gili, "Dielectric Spectroscopy of Erythrocyte Cell Suspensions. A Comparison between Looyenga and Maxwell-Wagner-Hanai Effective Medium Theory Formulations," Journal of Non-Crystalline Solids, vol. 305, pp. 278-284, 2002.

[9] K. Asami and T. Yamaguchi, "Electrical and Morphological Changes of Human Erythrocytes under High Hydrostatic Pressure followed by Dielectric Spectroscopy," Annals of Biomedical Engineering, vol. 27, pp. 427-435, 1999.

[10] P. Zoltowski, "On the Electrical Capacitance of Interfaces Exhibiting Constant Phase Element Behavior," Journal of Electroanalytical Chemistry, vol. 443, pp. 149-154, 1998.

[11] F. Jaspard and M. Nadi, "Dielectric Properties of Blood: an Investigation of Temperature Dependence," Physiological Measurement, vol. 23, pp. 547-554, 2002.

[12] L. Chin, M. Sherar, "Changes in Dielectric Properties of *Ex vivo* Bovine Liver at 915 MHz during Heating," Physics in Medicine and Biology, vol. 46, pp. 197-211, 2001.

[13] R. Pethig, "Dielectric Properties of Body Tissues" Clinical Physics and Physiological Measurement, vol. 8, pp. 5-12, 1987.

[14] H. Fricke, "The Electric Capacity of Suspensions of Red Corpuscles of a Dog," Physiology Review, vol. 26, pp. 682-687, 1925.

[15] H. Fricke, "The Electric Capacity of Suspensions with Special Reference to Blood," Journal of General Physiology, vol. 9, pp. 137-152, 1925.

[16] R. Hoeber, "Eine methode die elektrische leitfahigkeit im in nern von zellen zu messen," Arch. ges. Physiol., vol. 133, pp.237-259, 1910.

[17] R. Hoeber, "Ein zweites verfahren die leitfahigkeit im inner ¨von zellen zu messen," Arch. ges. physiol., vol. 148, pp. 189-221, 1912.

[18] H. P. Schwan and T. P. Bothwell, "Electrical Properties of the Plasma Membrane of Erythrocytes at Low Frequencies", Nature, vol. 178, pp. 265-266, 1956.

[19] H. P. Schwan and E. L. Carstensen, "Dielectric Properties of the Membrane of Lysed Erythrocytes," Science, vol. 125, pp. 985-986, 1957.

[20] H. P. Schwan, "Electrical Properties of Tissue and Cell Suspensions" Advances in Biological and Medical Physics, Academic Press, New York, vol. 5, pp. 147-209, 1957.

[21] K. R. Foster and H. P. Schwan, ''Dielectric Properties of Tissues and Biological Materials: A Critical Review'', Critical Review in Biomedical Engineering, vol. 17, pp. 25-104, 1989.

[22] C. Prodan, F. Mayo, J. R. Claycomb, J. H. Miller, Jr., and M. J. Benedik, "Low-Frequency, Low-Field Dielectric Spectroscopy of Living Cell Suspensions," Journal of Applied Physics, vol. 95, pp. 3754-3756, 2004.

[23] O. G. Martinse, S. Grimmes, and H. P. Schwan, "Interface Phenomena and Dielectric Properties of Biological Tissue," Encyclopedia of Surface and Colloid Science, E. Hubbard editor, New York: Marcel Dekker, pp. 2643-2652, 2002.

[24] R. D. Stoy, K. R. Foster, and H. P. Schwan, "Dielectric Properties of Mammalian Tissues from 0.1 to 100 MHz: a Summary of Recent Data," Physics in Medicine and Biology, vol. 27, pp. 501-513, 1982.

[25] K. Asami, "Characterization of Biological Cells by Dielectric Spectroscopy," Journal of Non-Crystalline Solids, vol. 305(1-3), pp. 268-277, 2002.

CHAPTER 4
Complex Permittivity Measurement

4.1 State of the Art

There are numerous ways of measuring complex permittivity at radio- and micro-wave frequencies [1-10]. The discussion herein will focus solely on methods relevant to the measurement of biological samples. Biological permittivity measurements are performed using one of four techniques: frequency and time domain spectrometry, network analysis, and coaxial line reflectrometry. Primarily, these techniques differ in the method of signal delivery to the sample. Recent research has been dominated by network analysis and coaxial line reflectrometry due to relevant technological advancements in material analyzer applications. Fig. 4.1 depicts three standard non-destructive probes often used to obtain the dielectric spectra of a biological sample: capacitive, inductive, and reflective [11].

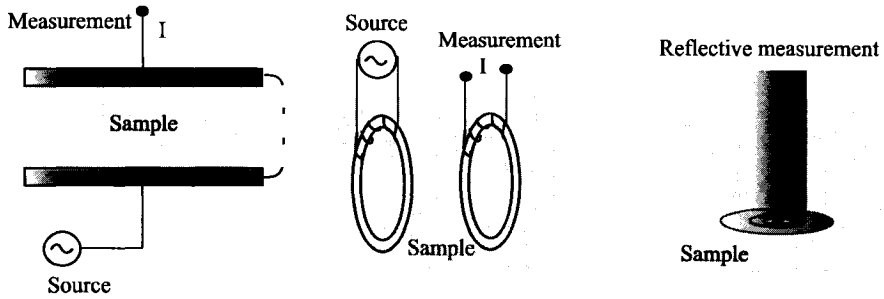

Figure 4.1. Permittivity measurement techniques. A) Capacitive method, B) inductive method, and C) reflective method.

The capacitive method uses the sample as a dielectric in between two or more electrodes. Since the distance in between the electrodes is fixed the capacitance will vary according to the permittivity of the sample. The capacitive plate geometry is most applicable to liquids since the full separation space is evenly filled. Although the method is effective, electrode contact with the sample is large resulting in undesired electrode polarization at low frequencies.

The inductive measurement technique employs two torroidal coils immersed in the sample. A variable voltage applied to one of the coils induces a current in the opposing coil proportional to the strength of the joining flux lines. Again, maintaining accurate sample alignment is difficult, it would be difficult to establish repeatable measurements for porous scaffolds.

The reflective method requires the application of an open-ended waveguide for the transmission of an electromagnetic (EM) wave onto the sample. The EM wave is usually generated and measured by a material analyzer. Permittivity is calculated by relating it to the measured echo signal (impedance, admittance, or reflection coefficient) of the sample interface through an appropriate electrical aperture model. The physical probe design has a geometry that is easily applicable to semi-solids, such as scaffolds, as well as liquids. Consequently, the reflective method is the most appropriate choice for this thesis.

4.2 Waveguides

Structures that guide the propagation of EM waves are referred to as waveguides. EM waves can propagate along hollow metal structures of arbitrary cross section. The guided EM wave can exhibit three kinds of distinct propagation modes: transverse electromagnetic (TEM) which has no field components in the direction of propagation (longitudinal direction), transverse magnetic (TM) which has a longitudinal electric field and transverse electric (TE) which has a longitudinal magnetic field. TM and TE modes have cutoff frequencies below which the EM wave can no longer propagate. Waveguides of a single conductor are incapable of supporting the TEM mode of propagation. Consequently, a single conductor waveguide functions like a high-pass filter with a characteristic cut off frequency. Circular and rectangular waveguides are examples of single conductor waveguides while a coaxial transmission line is a two-conductor waveguide. Waveguides have a dominant EM propagation mode that could be TEM, TM, or TE. With increasing frequency other propagation modes may be excited.

There are several techniques of performing a reflection measurement. Various waveguides can be implemented for the measurement. The first reflection measurements were performed with rectangular waveguides [12-14] and then with circular waveguides [15]. The limitation of these waveguides is their innate, characteristic, low frequency cut-off. High frequency limits of these waveguides are determined by the onset of higher order EM modes that complicate the EM aperture modeling of the waveguide probe. Furthermore, the frequency band of operation increases with the size of the single conductor waveguide. For practical application it is desirable for the probe to remain small and least intrusive.

4.3 Open-ended Coaxial Probe

Open-ended coaxial probes are an attractive alternative to single conductor waveguides because they allow measurement from DC up to 50 GHz [16]. Fabrication is relatively straightforward for they are very similar to coaxial adapters that are commercially available [17]. Also, broadband measurements can be performed with small coaxial probes using frequency and time-domain techniques.

Currently, open-ended coaxial probes are the most ubiquitous tools for measuring permittivity of biological media. They have been often applied for the non-destructive characterization of biological tissue, both *in vitro* [18-20] and *in vivo* [21-23], as well as in diagnostic devices for breast cancer and other sub-dermal diseases [24-26]. Their popularity has led to the development of many models for the aperture admittance of an open-ended coaxial probe. Also, numerous automated material analyzers that generate the EM signal and record the echo signal are now commercially available and easily interfaced with open-ended coaxial probes.

The geometry of an open-ended coaxial probe consists of an inner conductor of radius a with an outer conductor of radius b terminated with a conductive flange as depicted by Fig. 4.2. The space between the two conductors

is filled with a dielectric that exhibits stable dielectric properties throughout the range of the excitation field.

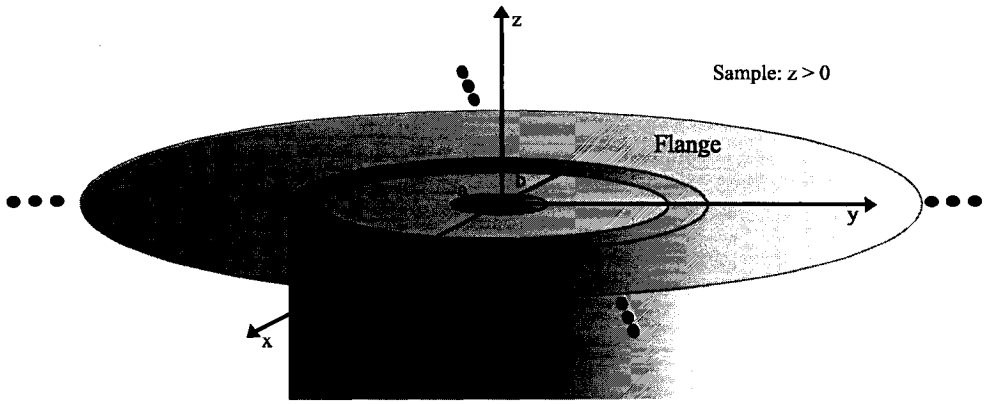

Figure 4.2. The coaxial probe and geometry of the problem

4.3.1 Modeling the Aperture Admittance

Estimating sample permittivity requires solving both the forward and inverse problems. The forward problem is that of relating the admittance of the probe aperture to sample permittivity. The forward problem formulation is the model of the probe's aperture admittance. The inverse problem is that of isolating the permittivity from the forward formulation. For simplicity, most aperture admittance models assume the sample: i) isotropic, ii) homogenous, iii) linear, iv) non-magnetic, and v) of infinite extent. Furthermore, most models assume that only the TEM dominant mode of light propagation is present. The validity of this assumption has been discussed in various works with differing opinions [27-29]. In general, for low frequency operation with a probe of large dimensions it is suggested that the effects of higher order EM propagation modes must be included for an accurate aperture model [16]. In this work higher order modes are not included in modeling because the aperture is small.

A robust method for solving the aperture admittance model based on solving an integral equation for the tangential electric field at the aperture was introduced by Mosig *et al* [30]. The technique matches the EM fields at the interface between the coaxial line and the biological tissue. An iterative technique can be applied to the method of Mosig *et al* to solve the inverse problem and

extract the permittivity. The method is highly accurate but requires extensive calculations and so is impractical for on-line application. Similarly, Nevels *et al* [31], Grant *et al* [32] and Delecki and Stuchly [33] presented rigorous analyses of the aperture admittance leading to accurate results but were inapplicable for an on-line application. Consequently, research was directed into producing a model for the aperture admittance that sacrifices certain accuracy for a simpler expression. Generally the expressions were simplified by focusing on a specific frequency range. Numerous such approximate techniques have been described over the years [34].

The most used models for application are those based on the formulation of Stuchly and Stuchly [34-39] and Misra *et al* [40-43]. Both models were considered for the current application. The Stuchly and Stuchly model consists of two capacitors in parallel as depicted by Fig. 4.3, where C_l accounts for fringing fields inside the coaxial line and C_0 is proportional to the permittivity of the sample.

$$Y_L = j\omega\varepsilon_0\varepsilon_l C_l + j\omega\varepsilon_0\varepsilon^*_{sample} C_0 \quad (S), \tag{4.1}$$

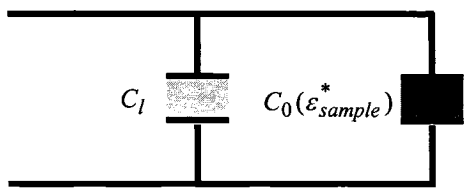

Figure 4.3. Electrical equivalent circuit of the Stuchly and Stuchly model [34-39]

Where ε_l and ε^*_{sample} are, respectively, the complex permittivity within the line and the permittivity of the sample. The values of the two capacitors must be determined experimentally using standards of known permittivity as presented in [37, 38]. The inverse problem is basically the isolation of the sample permittivity in (4.1). The Stuchly and Stuchly model was later expanded for further accuracy:

$$Y_L = K_1 + K_2\varepsilon^*_{sample} + K_3{\varepsilon^*_{sample}}^2 + K_4{\varepsilon^*_{sample}}^{2.5} \quad (S). \tag{4.2}$$

Where K_1, K_2, K_3, and K_4, are frequency dependant constants specific to probe geometry. Consequently, solving for the constants requires a precise knowledge of standard material properties. These models are valid for electrically small apertures [34].

Misra *et al* proposed a similar model for the aperture admittance composed of two capacitors and a parallel radiation conductance. The model is based on variational principles that are applied for determining characteristic quantities such as impedances. The variational technique is a stationary approximation to the desired quantity; which means that the formula is insensitive to variations in an assumed field about the correct field. A quasi-static approximation of the formulation integrand is used leading to the aperture admittance expression:

$$Y_L = \frac{j2k^2}{\omega\mu_0[\ln(\frac{b}{a})]^2}\int_a^b\int_a^b\int_0^\pi \frac{\cos(\phi')\exp(-jku)}{u}drdr'd\phi' \quad (S) \tag{4.3}$$

where

$$u = [r^2 + r'^2 - 2rr'\cos(\phi')]^{1/2}, \tag{4.4}$$

u_0 and k are, respectively, the permeability of free space and the wavenumber in the material medium, and a cylindrical coordinate system is assumed for the problem as depicted in Fig. 4.4.

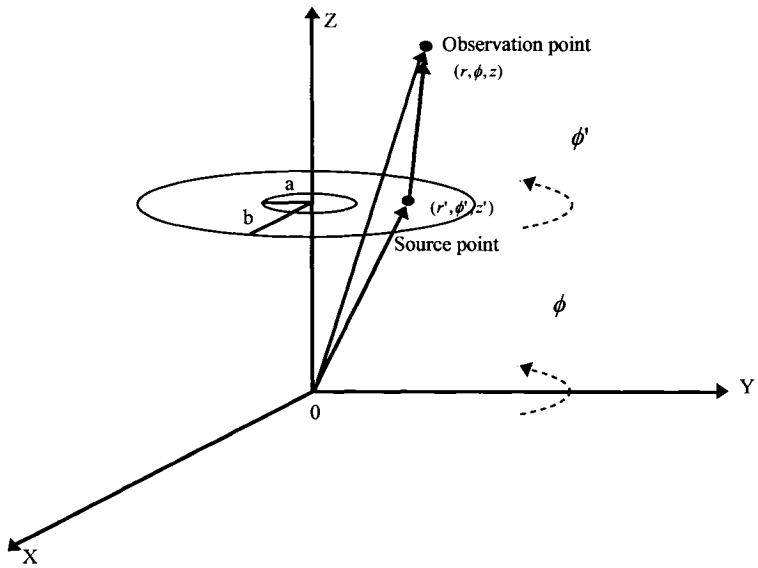

Figure 4.4. Detailed geometry for the model proposed by Misra *et al*

If the electrical opening is very small then the integral expression can be simplified to the first few terms of the exponential series expansion. It should be noted that the model (4.3) maps to (4.2) where K_1 is found to be zero:

$$Y_L = \frac{j2\omega I_1 \varepsilon_0}{[\ln(b/a)]^2}\varepsilon^*_{sample} - \frac{j\omega^3 \mu_0 I_2 \varepsilon_0^2}{[\ln(b/a)]^2}\varepsilon^{*2}_{sample} + \frac{\pi\omega^4 \mu_0^{1.5}[b^2 - a^2]^2 \varepsilon_0^{2.5}}{12[\ln(b/a)]^2}\varepsilon^{*2.5}_{sample} \quad (S) \tag{4.5}$$

where

$$I_1 = \int_a^b \int_a^b \int_0^\pi \frac{\cos(\phi')}{\sqrt{r^2 + r'^2 - 2rr'\cos(\phi')}} d\phi' dr dr', \tag{4.6}$$

$$I_2 = \int_a^b \int_a^b \int_0^\pi \cos(\phi)\sqrt{r^2 + r'^2 - 2rr'\cos(\phi')}\, d\phi' dr dr', \tag{4.7}$$

Knowing the exact dimensions of the probe one can solve for the remaining constants producing an expression for the admittance as a function of sample permittivity.

The inverse problem becomes much simpler under some specific conditions. In particular, at low frequencies and for high values of the sample permittivity modulus only K_2 needs to be retained in the aperture admittance expression of (4.5):

$$\varepsilon^*_{sample} = -j\frac{Y_L\left[\ln\left(b/a\right)\right]^2}{2\omega\varepsilon_0 I_1}. \tag{4.8}$$

Given the generally high modulus of biological media at low frequencies this simplified expression was deemed to be most appropriate for the current on-line application.

4.3.2 Calibration and Error Correction

There are often discrepancies between experimental and theoretical permittivity results. At high frequencies, the omission of higher order EM propagation modes for most aperture admittance models produces inaccuracies. The effects of this phenomena falls out of the frequency range of interest here. At

low frequencies, numerous media experience different characteristic dispersions causing uncertainty in the permittivity measurement [34]. Physical faults of the system setup such as scratched probe surfaces, bent conductors and cables, and bad connections between system components will influence measurements at all frequencies. Physical disturbance of the system during a measurement, such as surface vibrations, can also alter the measurement. An imperfect interface between the sample and probe will skew measurements; a frequent phenomenon is the accumulation of air bubbles at the probe surface when taking measurements of liquids; air has a very low permittivity ($\epsilon = 1$) and so can significantly skew results.

Measurement accuracy can be improved by proper calibration and error correction of the probe and material analyzer. The material analyzer is most often calibrated at the port that connects to the probe apparatus with a commercial calibration kit. The calibration measurements include an open-circuit, a short circuit, and a matched load. A second calibration needs to be performed at the probe's aperture. It is hard to achieve good calibration at the probe aperture because it is difficult to apply a matched load and an accurate short. The most common procedure for calibrating the probe is to first measure an open circuit by leaving the probe in air; then, emulate a short circuit by pressing aluminum foil against the probe surface assuring good contact between both conductors; finally measure a standard liquid, usually distilled water, having a well described theoretical permittivity behavior. These measurements are then used to solve for the parameters of an error model. The problem of using a standard liquid for calibration is its permittivity depends on factors such as temperature, atmospheric pressure, and ion concentration. Thus, it may be difficult to produce repeatable measurements given that each calibration can be slightly different. To improve the calibration, prior to any measurement the probe should always be washed and dried with a lint-free cloth to remove any particles that may alter the constitution of the sample. When measuring liquids, the probe should be gently tapped to dislodge any air bubbles that may be attached to the probe surface. Nonetheless

the standard deviations of the error between the theoretical and experimental measurements are reported to be as high as 4-15 % [16, 44].

4.4 Chapter Segue

This chapter introduced complex permittivity measurement by an open-ended coaxial probe. The physical probe, measurement methods, and the analytical modeling technique required to relate complex permittivity to a reflective measurement were presented. What remains is to relate complex permittivity of a seeded scaffold to the cells within it.

The following chapter discusses the various effective medium approximations (EMA) that model the seeded scaffold, or cell suspension, sample. It is the EMA that relates the sample constituents to a complex permittivity measurement.

4.5 References

[1] S. Roberts and A. A. Von Hippel, "A New Method for Measuring Dielectric Constant and Loss in the Range of Centimeter Waves," Journal of applied Physics, vol. 17, pp. 610-616, 1946.

[2] R. M. Redheffer, "The Measurement of Dielectric Constants," Technique of Microwave Measurements, C. G. Montgomery editor, McGraw-Hill Book Company, Inc., 1947.

[3] A. R. Von Hippel, "Dielectrics and Waves," New York: Wiley, 1954.

[4] D. M. Bowie and K. S. Kelleher, "Rapid Measurement of Dielectric Constant and Loss Tangent," IEEE Transactions Microwave Theory Technology, pp. 137-140, 1956.

[5] J. N. Bhar, "Microwave Techniques in the Study of Semiconductors," Proceedings of the IEEE, pp. 1623-1631, 1963.

[6] A. C. Lynch, "Precise Measurements on Dielectric and Magnetic Materials," IEEE Transactions on Instrumentation and Measurement, vol. IM-23, pp. 425-431, 1974

[7] P. Queffelec, P. Gelin, J. Gieraltowski, and J. Loaec, "A Microstrip Device for the Broad Band Simultaneous Measurement of Complex Permeability and Permittivity," IEEE Transactions on Magnetics. vol. 30, pp. 224-231, 1994.

[8] J. Krupka, K. Derzakowski, A. Abramowicz, M. E. Tobar, and R. G. Geyer, "Use of Whispering-Gallery Modes for Complex Permittivity Determinations of Ultra-Low-Loss Dielectric Materials," IEEE Transactions on Microwave Theory and Techniques, vol. 47, pp.752-759, 1999.

[9] R. Olmi, M. Bini, A. Ignesti and C. Riminesi, "Non-Destructive Permittivity Measurement of Solid Materials," Measurement Science and Techniques, vol. 11 pp. 1623-1629, 2000.

[10] E. Fratticcioli, M. Dionigi, and R. Sorrentino, "A Simple and Low-Cost Measurement System for the Complex Permittivity Characterization of Materials," IEEE Transactions on Instrumentation and Measurement, vol. 53, pp. 1071-1077, 2004.

[11] K. Asami, "Characterization of Heterogeneous Systems by Dielectric Spectroscopy," Progress in Polymer Science, vol. 27, pp. 1617-1659, 2002.

[12] J. Galejs and M. Mentzoni, "Waveguide Admittance for Radiation into Plasma Layers - Theory and Experiment," IEEE Transactions on Antennas and Propagation, vol. 15, pp. 465-470, 1967.

[13] A. T. Villeneuve, "Equivalent Circuits of Junctions of Slab-Loaded Rectangular Waveguides" IEEE Transactions on Microwave Theory and Techniques, vol. 33, pp. 1196 – 1203, 1985.

[14] W. Croswell, R. Rudduck, and D. Hatcher, "The Admittance of a Rectangular Waveguide Radiating Into a Dielectric Slab" IEEE Transactions on Antennas and Propagation, vol 15, pp. 627 – 633, 1967.

[15] M. C. Bailey and C. T. Swift, "Input Admittance of a Circular Waveguide Aperture Covered by a Dielectric Slab," IEEE Transaction on Antennas and Propagation, vol. AP-16, pp. 386-391.

[16] C. L. Pournaropoulos, "A Study on the Coaxial Aperture Electromagnetic Sensor and its Application in Material Characterization" PhD dissertation, The University of Wisconsin-Milwaukee, 1996.

[17] N. I. Sheen, and I. M. Woodhead, "An Open-ended Caoxial Probe for broad-band Permittivity Measurement of Agricultural Products," Journal of Agricultural Engineering, vol 74, pp. 193-202, 1999.

[18] R. D. Stoy, K. R. Foster and H. P. Schwan, "Dielectric Properties of Mammalian Tissues from 0.1 to 100 MHz: a Summary of Recent Data," Physics in Medicine and Biology, vol. 27, pp. 501-513, 1982.

[19] E. F. Treo, C. J. Felice, M. C. Tirado, M. E. Valentinuzzi, and D. O. Cervantes, "Hematocrit Measurement by Dielectric Spectroscopy," IEEE Transactions on Biomedical Engineering, vol. 52, pp. 124-127. 2005.

[20] C. Gabriel, S. Gabriely, and E. Corthout, "The Dielectric Properties of Biological Tissues: I. Literature Survey," Physics in Medicine and Biology, vol. 41, pp. 2231–2249, 1996.

[21] G. L. Hey-Shiptont, P. A. Matthews, and J. McStay, "The Complex Permittivity of Human Tissue at Microwave Frequencies," Physics in Medicine and Biology, vol. 27, pp. 1067-1071, 1982.

[22] M. A. Stuchly, A. Kraszewskit, S. S. Stuchly and A. M. Smith, "Dielectric Properties of Animal Tissues *In vivo* at Radio and Microwave Frequencies: Comparison Between Species," Physics in Medicine and Biology, vol. 27, pp. 927-936, 1982.

[23] M. Schaefer, K. Nowak, B. Kherad, W. Gross, S. Post, M. M. Gebhard, "Monitoring Water Content of Rat Lung Tissue *In vivo* Using Microwave Reflectometry," Medical and Biological Engineering and Computing, vol. 42, pp. 577-580, 2004.

[24] D. Popovic, L. McCartney, C. Beasley, M. Lazebnik, M. Okoniewski, S. C. Hagness, and J. H. Booske, "Precision Open-Ended Coaxial Probes for *In vivo* and *Ex vivo* Dielectric Spectroscopy of Biological Tissues at Microwave Frequencies," IEEE Transactions on Microwave Theory and Techniques, vol. 53, pp. 1713-1722, 2005.

[25] S. C. Hagness, A. Taflove, and J. E. Bridges, "Two-Dimensional FDTD Analysis of a Pulsed Microwave Confocal System for Breast Cancer Detection: Fixed-Focus and Antenna-Array Sensors," IEEE Transactions on Biomedical Engineering, vol. 45, pp. 1470-1479, 1998.

[26] E. C. Fear and M. A. Stuchly, "Microwave Detection of Breast Cancer," IEEE Transactions on Microwave Theory and Techniques, vol. 48, pp. 1854-1863, 2000.

[27] E. P. Irzinski, "The Input Admittance of a TEM Excited Annular Slot Antenna," IEEE Transaction on Antennas and Propagation, vol. 23, pp. 829-834, 1975.

[28] D. C. Chang, "Input Admittance and Complete Near-Field Distribution of an Annular Aperture Antenna Driven by a Coaxial Line," IEEE Transactions on Antennas and Propagation vol. 18, pp. 610-616, 1970.

[29] C. W. Harrison Jr., and D. C. Chang, "Theory of the Annular Slot Antenna Based on Duality," IEEE Transactions on Electromagnetic Compatibility, vol. 13, pp. 8-14, 1971.

[30] J. R. Mosig, J. E. Besson, M. Gex-Fabry and F. E. Gardiol, "Reflection of an Open-Ended Coaxial Line and Application to Nondestructive Measurement of Materials," IEEE Transactions on Instrumentation and Measurement, vol. 30, pp. 46-51, 1981.

[31] R. D. Nevels, C. M. Butler and W. Yablon, "The Annular Slot Antenna in a Lossy Biological Medium IEEE Transactions on Microwave Theory and Techniques, vol. 33, pp. 314-319, 1985.

[32] J. P. Grant, R. N. Clarke, G. T. Symm, and N. M. Spyrou, "A Critical Study of the Open-Ended Coaxial Line Sensor Technique for RF and Microwave Complex Permittivity Measurements" Journal of Physics E: Scientific Instruments, vol. 22, pp. 757-770, 1989.

[33] Z. A. Delecki, and S. S. Stuchly, "Analysis of the Open-Ended Coaxial Line Sensors," Journal of Electromagnetic Waves and Applications, vol. 4, pp. 169-183, 1990.

[34] C. L. Pournaropoulos and D. K. Misra, "The Co-axial Aperture Electromagnetic Sensor and its Application in Material Characterization," Measurement Science Technology, vol. 8, pp. 1191–1202, 1997.

[35] M. A. Stuchly and S. S. Stuchly, "Coaxial Line Reflection Methods for Measuring Dielectric Properties of Biological Substances at Radio and Microwave Frequencies – a Review" IEEE Transactions on Instrumentation and Measurement, vol. 29, pp. 176-183, 1980.

[36] M. M. Brady, S. A. Symons, and S. S. Stuchly, "Dielectric Behavior of Selected Animal Tissues *In vitro* at Frequencies from 2 to 4 GHz," IEEE Transactions on Biomedical Engineering, vol. 28, pp. 305–307, 1981.

[37] T. W. Athey, M. A. Stuchly, and S. S. Stuchly, "Measurement of Radio Frequency Permittivity of Biological Tissues with an Open-Ended Coaxial Line: Part I," IEEE Transaction on Microwave Theory and Technology, vol. 30, pp. 82-86, 1982.

[38] M. A. Stuchly, T. W. Athey, G. M. Samaras, and G. E. Taylor, "Measurement of Radio Frequency Permittivity of Biological Tissues with an Open-Ended Coaxial Line: Part II – Experimental Results," IEEE

Transactions on Microwave Theory and Technology, vol. 30, pp. 87–92, 1982.

[39] M. A. Stuchly, M. M. Brady, S. S. Stuchly and G. B. Gajda, "Equivalent Circuit of an Open-Ended Coaxial Line in a Lossy Dielectric," IEEE Transactions on Instrumentation and Measurement, vol. 31, pp. 116–119.

[40] C. L. Pournaropoulos and D. K. Misra, "A Study on the Coaxial Aperture Electromagnetic Sensor and its Application in Material Characterization," IEEE Transactions on Instrumentation and Measurement, vol. 43, pp. 111–115, 1994.

[41] D. K. Misra and J. A. McKelvey, "A Quasistatic Method for the Characterization of Stratified Dielectric Materials using an Open-Ended Coaxial Probe," Microwave Optic Technology, vol. 7, pp. 650–653, 1994.

[42] D. K. Misra, "On the Measurement of the Complex Permittivity of Materials by an Open-Ended Coaxial Probe," IEEE Microwave Guided Wave Letters, vol. 5, pp. 161–163. 1995.

[43] D. K. Misra, "Evaluation of the Complex Permittivity of Layered Dielectric Materials with the use of an Open-Ended Coaxial Line," Microwave Optic Technology Letters, vol. 11, pp. 183–187, 1996.

[44] G. P. Otto and W. C. Chew, "Improved Calibration of a Large Open-Ended Coaxial Probe for Dielectric Measurements," IEEE Transactions on Instrumentation and Measurement, vol. 40, pp. 742–746, 1991.

CHAPTER 5

Cell Concentration Measurement via Permittivity

5.1 Effective Medium Theory

In this thesis there is a need for an effective medium approximation (EMA) that describes the permittivity of a macroscopically inhomogeneous media. All EMAs are based on Maxwell's equations for the static limit [1] which describe interfacial polarization mechanisms. The first EMA formulation, proposed by Bruggeman [2], related a two-phase composite with the micro-geometry of the composite, i.e., the EMA formulation defined the effective permittivity, or conductivity, of the system as a function of the constituents from both phases. This paradigm has been extended to various studies of macroscopically inhomogeneous media including multi-phase composites. EMAs have been used to characterize heterogeneous systems such as particle suspensions, membranes in liquids, and other composite materials [3-8].

5.1.1 Cell Suspension EMA

A biological cell suspension is a heterogeneous system that has been investigated over the past century [6] and is most relevant to the current application. To model the effective permittivity response, the permittivity response of each system phase – the cells and ambient solution – must be combined. It must be stressed that the simple linear superposition of the dielectric expressions of each phase does not describe the effects of polarization. Consequently, the numerous approaches to describe the permittivity behavior of a cell suspension have been based on effective medium theory [6-8]. Most EMA formulations are defined by the bulk properties of the suspension:

$$f(\varepsilon^*_{eff}(\omega), \varepsilon^*_m(\omega), \varepsilon^*_{ck}(\omega), \varphi_{ck}) = 0, \tag{5.1}$$

where $\varepsilon^*_{eff}(\omega), \varepsilon^*_m(\omega), \varepsilon^*_{ck}(\omega)$ are, respectively, the effective, host medium complex permittivity (CP); while ε^*_{ck} and φ_{ck} are the CP and volume fraction of the k^{th} type of inclusion.

In the case of a cell suspension, there is only one type of inclusion, the cells, while the host medium is the cell medium. Note that these formulations do not account for interactions between the inclusions themselves. For low volume fractions of inclusions EMA formulations with the structure of (5.1) produce very similar results. Discrepancies begin to appear when the interactions between the particles can no longer be ignored or the polarizability of a single particle is very large.

In general, the unknowns of the EMA formulations are the parameters of the inclusions. The ambient permittivity measurement is that of the medium less the inclusions. For the single shell model (3.10) the unknowns are the conductivity and permittivity of the membrane and the cytoplasm. These unknowns may be estimated by using a non-linear fitting algorithm to relate the measured effective permittivity to the EMA.

Most EMA formulations assume an even inclusion organization throughout the ambient medium. In reality clusters of inclusions often form and inclusions are not all of the same volume or shape. However, on a macroscopic scale the mixture must be homogenous. Also, since the EMA is based on a static solution of the potential around an inclusion of specified permittivity it must be assumed that the inclusions are much smaller than the EM wavelength in the ambient medium. This is true for cell suspension measurements at radio- and micro-wave frequencies.

A recent review presented a coherent list of the numerous EMAs available for the modeling of heterogeneous systems [3]. Three EMAs that have been previously applied for cell suspensions and seeded scaffolds, the Maxwell-Wagner-Hanai, Looyenga, and Hanai functions will be discussed here.

5.1.2 *Maxwell-Wagner-Hanai Effective Medium Formulation*

The Maxwell-Wagner-Hanai formulation for a heterogeneous system as presented in [6] is:

$$\frac{\varepsilon_{eff}^{*}(\omega)-\varepsilon_{m}^{*}(\omega)}{\varepsilon_{eff}^{*}(\omega)+2\varepsilon_{m}^{*}(\omega)}=\sum_{k}\varphi\frac{\varepsilon_{ck}^{*}(\omega)-\varepsilon_{m}^{*}(\omega)}{\varepsilon_{ck}^{*}(\omega)+2\varepsilon_{m}^{*}(\omega)} \tag{5.2}$$

The formulation is based on the original Maxwell-Wagner derivation described previously (3.11). This EMA assumes a spherical cell model composed of two phases as described by (3.10). The model has been successfully applied to suspensions of erythrocytes and macrophages [6, 9]. Its accuracy was found to be highly dependent on the cell volume fraction; at high cell concentrations it produces innacurate results.

5.1.3 *Looyenga Effective Medium Formulation*

The Looyenga formulation for a heterogeneous system of small to moderate cell volume is:

$$\varepsilon_{eff}^{*}(\omega)=\left\{\sum_{k}\left(\varepsilon_{ck}^{*1/3}(\omega)-\varepsilon_{m}^{*1/3}(\omega)\right)p_{k}+\varepsilon_{m}^{*1/3}(\omega)\right\}^{3}. \tag{5.3}$$

This derivation makes no assumption as to the shape of the inclusions and is therefore applicable to any inclusion geometry. However, if the assumed cell model is spherical but the actual cells are not, the formulation does not fit the empirical permittivity data well. In addition, the formula breaks down as the ambient and inclusion permittivity become very distinct. Nonetheless, the formulation produces excellent fits for various heterogeneous suspensions [6,10]. A comparison between the Maxwell-Wagner-Hanai and Looyenga formulation for the measurement of Erythrocytes showed the Looyenga EMA formulation to be more accurate [6].

The Looyenga function was used by Bagnaninchi *et al* [9] to determine the porosity of scaffolds. The ambient measurement was ethanol, and the effective measurement was the micro-porous scaffold immersed in ethanol. The results were accurate within 2 % of porosity as calculated from the physical properties of the scaffold. The Looyenga function was used for the porosity calculation since

the microstructure of the scaffold was random and the formulation requires no assumption are about the shape of the inclusions.

5.1.4 Hanai Formulation

Hanai [11] extended the EMA formulation for suspended ellipsoids, first proposed by Bruggeman, to allow for high volume fractions of inclusions. His robust formulation conveniently simplifies under the assumption that the interfacial polarization dipole is in parallel with the applied electric field [3]. This derivation, presented by Boyle [12], who showed that the function's dependence on the depolarization factor n is related to the morphology of the suspended particle:

$$(1-\varphi)=\left(\frac{\varepsilon^*_{eff}(\omega)-\varepsilon^*_{cell}(\omega)}{\varepsilon^*_{m}(\omega)-\varepsilon^*_{cell}(\omega)}\right)\left(\frac{\varepsilon^*_{m}(\omega)}{\varepsilon^*_{eff}(\omega)}\right)^{n}. \tag{5.4}$$

The depolarization factor has three designated values for different morphologies: i) n = 1/3 for spherical inclusions, ii) n = 1/2 for cylinders whose longitudinal direction is perpendicular to the direction of the electric field and iii) n = 1 for a two-planar system associated with a lamellar cell morphology.

The Hanai function and its variations have been successfully implemented for modeling the effective permittivity of cell suspensions of various concentrations of erythrocytes [3], macrophages [9], and pre-ostoblasts [9]. As well, the Hanai function has been used to monitor the evolution of cell morphology as cells adhered to the surface of the open-ended coaxial probe over a period of time [9]. The Hanai function was chosen for this work because it performs accurately irrespective of volume fraction and simplifies when a lamellar cell shape is assumed – attached pre-osteoblasts are lamellar.

5.1.5 Cell Models

The EMA theory requires a description of the cell permittivity. Given that the cell is a complex heterogenous structure a simplified model must be assumed, such as the single shell model introduced by J. C. Maxwell and K. W. Wagner. There are numerous cell models that assume different morphology and number of

permittivity phases. Most cell models assume a particle of a particular shape enveloped by a layer between its surface and the external medium. However, multi-shell cell models [3] are being explored that may account for the lipid bilayer of cell membranes. Cell models are formulated by solving the Laplace equations under the boundary conditions at the interfacing surfaces [13-15]. Once the cell has been modeled it can be applied in any EMA. However, certain EMA formulations are tailored for a specific cell model.

5.2 Past Work on Scaffold Cell Concentration Measurement

The initial stage of this research, presented by Bagnaninchi *et al* in [16], introduced the concept of permittivity measurement for monitoring tissue growth. Permittivity measurements were performed with a commercial system rated for frequencies greater than 200 MHz.

5.2.1 Porosity Measurement

First, effective measurements were performed on empty scaffolds immersed in 100 % ethanol to demonstrate that the porosity of the scaffold could be measured with the Looyenga EMA. In this case the inclusions where considered to be the scaffold itself. The ambient (control) measurement was 100 % ethanol. The measurements were performed over a frequency range of 200-2000 MHz. The estimated porosity was within 2 % of the calculated porosity based on the chitosan density, sample volume, and weight [9].

5.2.2 Cell Suspension Measurement

The next step was to test the system with cell suspensions of different known concentrations. Cell suspensions of mouse monocyte-macrophages were prepared in two different concentrations: 3.1 million cells/ml and 1.6 million cells/ml. The permittivity of the suspensions were measured from 200-1200 MHz under sterile conditions. The Maxwell-Wagner-Hanai EMA function was used to relate the cell parameters to the measured effective permittivity. The estimated

cell constituent values corresponded to the real values, and the recorded cell concentrations were within 1% of the true values [9].

5.2.3 Scaffold Cell Concentration Variation

The system was then applied to measure the cell concentration in scaffolds of different cell concentrations. Scaffolds seeded with 1, 1.2, and 1.5 million macrophages/ml were measured in the same manner as the suspensions. The control measurement was that of an empty scaffold in the applied cell medium. The system produced accurate relative cell concentration measurements for the three sets of scaffolds [9]. However, the absolute cell concentration measurements overestimated the actual seeded cell concentration. This error was attributed to the accumulation of cells on the scaffold side of seeding which acted as the bio-interface between the probe and sample.

The system response to a scaffold with a different cell-line was analyzed. Two sets of scaffolds seeded with 1 and 2 million pre-osteoblast cells were measured by the system; however, the Hanai function was used as the EMA, a lamellar shape was assumed for the attached cells, and the lower limit of the applied frequency range was set to 100 MHz. The ambient measurement was a non-seeded scaffold immersed in the applied cell medium. As with the measurements of the seeded macrophages, the system produced accurate relative measurements but the absolute concentration results overestimated the true values [17].

5.2.4 Scaffold Cell Injections

The same system was used to record the progressive cell volume fraction change in a scaffold injected with 0.2 million cells every 3 minutes up to a total cell count of 1.6 million. The cell injections significantly lowered the loss factor of the measured permittivity as expected from the EMA theory of cell suspensions. The corresponding cell concentration curve was linear for the first 4 injections. However, for the last four injections the system did not detect a

significant cell concentration change because the added cell numbers now constituted a cell volume fraction too low for detection.

5.2.5 Cell Signature

The cell signature vector was defined as the real permittivity of the cell membrane (ε'_{mem}), the real permittivity of the cytoplasm (ε'_{cyt}), and the conductivity of the cytoplasm (σ_{cyt}). These parameters were retrieved for macrophages and pre-osteoblasts and are reproduced in Table 5.1 for convenience. The detected cell signature was significantly different for the two cell lines. Indicating that the system could discriminate between cell lines.

Table 5.1. Cell signature parameters retrieved from permittivity measurements of cell seeded scaffolds [17].

	ε'_{mem}		ε'_{cyt}		σ_{cyt}	
	mean	std dev	mean	std dev	mean	std dev
Pre-ostoeblasts	32.09	11.69	85.96	4.73	0.24	0.11
Macrophages	4.50	0.13	71.07	0.38	0.20	0.00

5.2.6 Cell Proliferation and Differentiation

Application of the system for cell proliferation and differentiation measurement was explored using two batches of seeded scaffolds. Batch 1 was seeded with 0.75 million cells and cultured in differentiation medium. Batch 2 was seeded with 0.4 million cells and cultured in regular medium. The scaffolds were monitored over a 12 day period with permittivity measurements done every second day. A DNA assay (CyQuant) was used for validation.

The relative cell concentration curve of batch 2 corresponded well to that of the DNA assay. However, the relative cell concentration curve of batch 1 recorded a plateau of cell growth after six days where the DNA assay recorded growth. It was hypothesized that since batch 1 was cultured in differentiation medium, which promotes significant formation of well-mineralized extra-cellular matrix (ECM), the permittivity measurement was modified by the presence of ECM.

5.2.7 Research Segue

There were three issues with this experimental procedure. First, only a single scaffold was sacrificed for each DNA assay prohibiting any statistical analysis. Second, the real permittivity appeared to be corrupt at frequencies below 200 MHz. Finally, the frequency range of permittivity measurement only overlapped the frequency range of the β-dispersion slightly. Consequently the system was not highly responsive to cell concentration variation.

The experiments and methodology presented in this thesis are motivated by these issues. We have designed a system to function at lower frequencies to provide greater sensitivity to changes in cell concentration within the scaffold. The experiments performed were robust to permit statistical analysis and to provide a standard for comparison of future measurements. Furthermore, the work focused on presenting a cohesive description of the system's modules. All system elements are presented and discussed to facilitate its reproduction and implementation as a tool for other research into tissue growth measurement within micro-porous scaffolds.

5.3 Chapter Segue

This chapter introduced the application of an EMA that estimates the cell signature and concentration of a seeded scaffold. Different EMAs and their approximations were reviewed. Past work was described to present the motivation and need for this thesis. Here, all the elements of the system were reviewed.

The following chapter is a manuscript for submission to an appropriate journal that presents a nondestructive system for the measurement of cell concentration within micro-porous scaffolds. The manuscript consolidates the information presented in the prior chapters, and describes the system in depth, and validates its performance.

5.4 References

[1] D. Stroud, "The Effective Medium Approximations: Some Recent Developments," Superlattices and Microstructures, vol. 23, pp. 567-573, 1998.

[2] D. A. G. Bruggeman, "Berechnug Vershiedener Physikalischen Konstanten von Heterogenen Substanzen,". Ann. Phys., vol. 24, pp. 636-664, 1935.

[3] K. Asami, "Characterization of Heterogeneous Systems by Dielectric Spectroscopy," Progress in Polymer Science, vol. 27, pp. 1617-1659, 2002.

[4] K. Asami, T. Yonezawa, "Dielectric Behavior of Non-Spherical Cells in Culture," Biochimica et Biophysica Acta, vol. 1245, pp. 317–324, 1995.

[5] F. Bordi, C. Cametti, Rosi, and A. Calcabrini, "Frequency Domain Electrical Conductivity Measurements of the Passive Electrical Properties of Human Lymphocytes," Biochimica et Biophysica Acta, vol. 1153, pp. 77–88, 1993.

[6] F. Bordi, C. Cametti, and T. Gili, "Dielectric Spectroscopy of Erythrocyte Cell Suspensions. A Comparison between Looyenga and Maxwell-Wagner-Hanai Effective Medium Theory Formulations," Journal of Non-Crystalline Solids, vol. 305, pp. 278-284, 2002.

[7] K. Asami, "Characterization of Biological Cells by Dielectric Spectroscopy," Journal of Non-Crystalline Solids, vol. 305, pp. 268–277, 2002.

[8] R. Pethig, "Dielectric and Electronic Properties of Biological Materials," New York: Wiley, 1979.

[9] P. O. Bagnaninchi, M. Dikeakos, T. Veres, and M. Tabrizian, "Towards On-line Monitoring of Cell Growth in Microporous Scaffolds: Utilization and Interpretation of Complex Permittivity Measurements," Biotechnology and Bioengineering, vol. 84, pp. 343-350, 2003.

[10] W. M. Merrill, R. E. Diaz, M. M. LoRe, M. C. Squires, and N. G. Alexopoulos, Effective Medium Theories for Artificial Materials Composed of Multiple Sizes of Spherical Inclusions in a Host Continuum," IEEE Transactions on Antennas and Propagation, vol. 47, pp. 142-148, 1999.

[11] T. Hanai, "Theory of the Dielectric Dispersion due to the Interfacial Polarization and its Application to Emulsion," Kolloid-Z, vol. 171. pp. 23–31, 1960.

[12] M. H. Boyle, "The Electrical Properties of Heterogeneous Mixtures Containing an Oriented Spheroidal Dispersed Phase," Colloid and Polymer Science 1985, vol. 263, pp. 51–57.

[13] K. Asami, T. Hanai, N. Koizumi "Dielectric Approach to Suspensions of Ellipsoidal Particles Covered with a shell in Particular Reference to Biological Cells," Japan Journal of Applied Physics, vol.19, pp. 359-365, 1980.

[14] G. Schwarz, M. Saito, and H. P. Schwan, "On the Orientation of Nonspherical Particles in an Alternating Electrical Field. Journal of Chemistry and Physics, vol. 10, pp. 3562–3659, 1965.

[15] M. Saito, H. P. Schwan, and G. Schwarz, "Response of Nonspherical Biological Particles to Alternating Electric Fields," Journal of Biophysics, vol. 6, pp. 313-327, 1966.

[16] P. O. Bagnaninchi, M. Dikeakos, T. Veres, and M. Tabrizian, "Monitoring of Stem Cell Proliferation and Differentiation using a Permittivity Responsive Biointerface," Materials Research Society Symposium Proceedings, vol. 773, pp. N7.12.1, 2003.

[17] P. O. Bagnaninchi, M. Dikeakos, T. Veres, and M. Tabrizian, "Complex Permittivity Measurement as a New Non-invasive Tool for Monitoring *In-vitro* Tissue Engineering and Cell Signature Through the Detection of Cell Proliferation, Differentiation, and Pre-tissue Formation," IEEE Transactions on Nanobioscience, vol. 3, pp. 243-250, 2004.

CHAPTER 6
Proposed System for Tissue Growth Monitoring

NONDESTRUCTIVE ON-LINE *IN-VITRO* MONITORING OF PRE-OSTEOBLAST CELL PROLIFERATION WITHIN MICRO-POROUS POLYMER SCAFFOLDS

D. Dziong[1], P. Bagnaninchi[2], R.E. Kearney[1], M. Tabrizian[1]

[1]McGill University, Montreal, Canada;

[2]Keele University, Keele, United Kingdom.

6.1 Abstract

We present a system for the on-line, *in-vitro*, nondestructive monitoring of tissue growth within micro-porous polymer scaffolds. The system is based on measuring the admittance of the sample over a frequency range of 10 – 200 MHz using an open-ended coaxial probe and impedance analyzer. The sample admittance is related to the sample complex permittivity (CP) by a quasi-static model of the probe's aperture admittance. A modified effective medium approximation is then used to relate the CP to the cell volume fraction. The change of cell volume fraction is used as a measure of tissue growth inside the scaffold.

The system detected relative cell concentration differences between micro-porous polymer scaffolds seeded with 0.4, 0.45, 0.5 and 0.6 × 10^6 pre-osteoblast cells. In addition, the pre-osteoblast proliferation within 56 scaffolds over 14 days was recorded by the system and a concurrent DNA assay. Both techniques produced cell proliferation curves that corresponded to those found in literature. Thus, our data confirmed that the new system can assess relative cell concentration differences in micro-porous scaffolds enabling on-line nondestructive tissue growth monitoring.

6.2 Introduction

Tissue engineering is based on seeding an organ-specific cell line onto a scaffold *in vitro* to cultivate tissue with a predefined shape [1,2]. The aim is to produce autologous tissue substitutes for implantation; achieving this goal would diminish problems of site scarcity, immune rejection, and pathogen transfer [3]. Although in its infancy, tissue engineering applications are expanding quickly due to concurrent advancements in biomaterials technology and stem cell research. Consequently, there is a need for new diagnostic devices and methods that will facilitate research and bring products to clinical application.

The major problem in tissue engineering is the design and construction of the scaffold that hosts the harvested cells [4]. Micro-porous polymer scaffolds are a popular choice due to their malleability, high porosity, and surface chemistry that allows cell attachment, proliferation, and differentiation [5]. Once a scaffold is seeded, it is necessary to record cell proliferation, and differentiation in stem cell applications, to monitor the stages of tissue development and modify the cultivation environment correspondingly. Current methods of monitoring constituent variation within scaffolds are laborious and compromise the integrity of the sample [6-8].

Complex permittivity measurement (CPM) over radio-wave frequencies, also known as dielectric spectroscopy, has been shown to be an excellent, non-destructive tool for monitoring cell growth in culture [9,10]. CPM has also become accepted as a diagnostic tool in industrial and medical bioprocesses [9,11,12]. Specifically, the use of open-ended coaxial probes as dielectric sensors has become ubiquitous because of their convenient geometry and well developed methods for extracting the CPM from the impedance measurement [13]. Consequently, dielectric probes and automated equipment that facilitates wide spectrum measurement of dynamic time-dependant phenomena in biological tissue, have become commercially available.

In previous work [14-16], we presented a novel methodology, based on CPM technology, for evaluating tissue growth within micro-porous polymer

scaffolds. The method detected differences in cell concentration in scaffolds, scaffold porosity, and stem cell differentiation within the scaffold. However, the formation of cell side-products, such as the ECM, resulted in underestimates of the cell concentration. Furthermore, below 200 MHz, where CPM is most sensitive to changes in cell concentration, the real part of CPM deviated significantly from theoretical behavior.

Here we present a comprehensive description of a system for the non-destructive measurement of tissue growth within micro-porous scaffolds based solely on the imaginary part of the CPM. Consequently, the system function works well in the frequency range of 10-200 MHz for greater response in cell concentration measurement. The individual elements of the system are presented along with suggested calibration methods. In this work, we implemented the probe aperture admittance model and error correction ourselves to present a coherent system for online measurement of cell concentration in micro-porous scaffolds. The performance of the system was evaluated by testing its ability to discriminate between scaffolds seeded with incrementally greater cell concentrations. Furthermore, the application of the system as a tool for cell proliferation was demonstrated by using it to monitor cell concentration variation in scaffolds over a period of 14 days and validate the results by a DNA assay and SEM analysis.

This note begins with a brief overview of CP theory related to the system. Then, the physical system setup is discussed with focus on each element. Subsequently, the mathematical modeling and other analytical techniques are presented followed by a description of scaffold construction and corresponding cell seeding. Last, experiments and a discussion of their results are presented together followed by a system summary and conclusion.

6.3 Theory

Complex permittivity (CP) describes a substance's reaction to an applied electric field. The real part of CP describes the amount of energy stored in the

material, while the imaginary part, the loss factor, is a measure of how dissipative the material is:

$$\varepsilon^*(\omega) = \varepsilon'(\omega) - j\varepsilon''(\omega), \tag{6.1}$$

where ω is the angular frequency of the excitation field, $\varepsilon'(\omega)$ and $\varepsilon''(\omega)$ are, respectively, the real and imaginary parts of CP.

There are two major responses when an electric field is applied to biological media: ion displacement and volume density polarization, also known as orientational polarization, oriented to neutralize the applied electric field. This polarization process is causal with a time constant characteristic of the medium. As the frequency of electric field variation increases the polarization vector falls out of phase with it. The loss factor describes the frequency dependent phase difference between electric field and the polarization vector. In addition, the loss factor accounts for ohmic losses due to ion displacement:

$$\varepsilon'' = \frac{\sigma_S + \sigma_D}{\varepsilon_0 \omega} = \frac{\sigma}{\varepsilon_0 \omega}, \tag{6.2}$$

where, σ_S, σ_D and ε_0 are, respectively, the static (ionic) and dynamic (orientational) conductivity and the permittivity of free space.

The dielectric spectrum of a cell suspension, or a seeded scaffold, is a function of both the cell structure and their environment. The cell structure can be modeled as a low conducting plasma membrane enveloping a conducting aqueous ionic medium, the cytoplasm [9]. While the environment is largely an ionic conducting cell medium.

Consequently, from an electrical viewpoint, the system can be considered to be a suspension of small capacitors, representing cells, in parallel with a resistive path, the cell medium [17]. The corresponding dielectric spectrum is a function of the capacitance of the system and therefore exhibits low pass filter behavior. The transition between the upper and lower plateau of the dielectric spectrum, over a frequency range of 1 Hz – 10 GHz is ideally characterized by four dispersions: α, β, δ and γ. The α-dispersion, although not well understood, is associated with the cellular membrane potential, sarcoplasmic reticulum polarization, gap junctions, and the displacement of counter ions surrounding

charged membranes and occurs at frequencies below approximately 5 kHz. The β-dispersion is most prominent and is due to the interfacial polarization between the plasma membrane and the intra- and extra-cellular ionic solutions, a phenomenon known as the Maxwell-Wagner effect which increases with cell volume and is most prominent at frequencies between 0.05 - 100 MHz. The α-dispersion is related to biopolymers, proteins, protein-bound water, and cell organelles and is observed between frequencies of 1 M – 1 GHz. The γ-dispersion is due to reorientation of water molecules and occurs at frequencies above 1 GHz.

Dielectric spectroscopy of cell suspensions has focused on the β-dispersion from which information about the sample constituents is extracted using an appropriate effective medium approximation (EMA). The EMA describes the relation of dielectric spectrum to the bulk properties of the sample. Its general form is [18]:

$$f(\varepsilon^*_{eff}(\omega), \varepsilon^*_m(\omega), \varepsilon^*_k(\omega), \varphi_k) = 0, \tag{6.3}$$

where,

$\varepsilon^*_{eff}(\omega)$: effective CP,

$\varepsilon^*_m(\omega)$: ambient medium CP,

$\varepsilon^*_k(\omega)$: the CP of the k_{th} inclusion CP,

φ_k : volume fraction of the k_{th} inclusions ,

ω : is the angular frequency in radians.

There are numerous EMAs that follow the formulation of (6.3) and produce substantially equivalent results [18]. In all cases, the EMA assumes an even distribution of inclusions throughout the sample. A sensitivity analysis of these EMA shows that the sensitivity of the effective CP to inclusion concentration increases at the lower end of the β-dispersion frequencies [16].

CPM of biological solutions at low frequencies is prone to corruption by electrode polarization due to the solution's high ionic content. At low frequencies,

the free ions in solution have time to accumulate at the electrode/sample interface creating an electrical double layer that increases the capacitance [19]. Numerous methods have been proposed to deal with this phenomenon; particular attention has been given to applying a power-law frequency dependence exhibiting a constant phase element to model polarization associated with open-ended coaxial probes [18,19]. However, including this term increases the complexity of the EMA formulation. Consequently, we chose a frequency range of 10 – 200 MHz for our system. This frequency range overlaps the β-dispersion of the cells but the loss factor is only minimally affected by the polarization phenomena and allows for discrimination between the static and dynamic conductivities. Fig. 6.1 shows the spectrum of an EMA for differing cell concentrations over this frequency range. Fig. 6.1A shows the tail-end of the β-dispersion shifting to lower frequencies with decreasing cell concentration. Fig. 6.1B shows the loss factor decreasing progressively with increasing cell concentration.

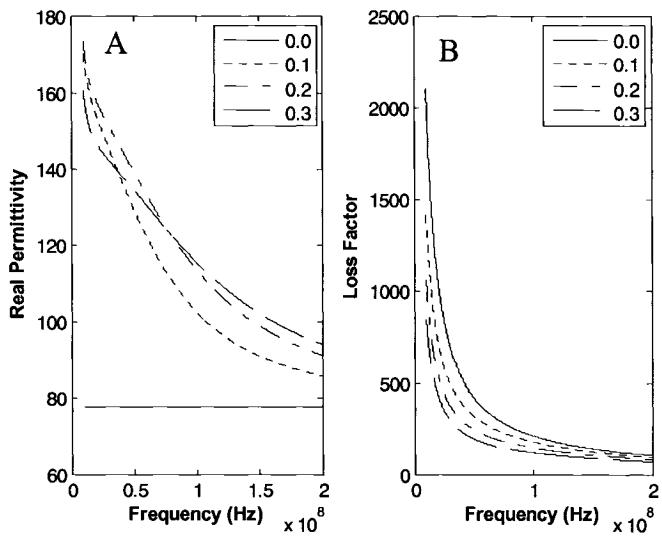

Figure 6.1. The theoretical dielectric spectra, as per the Hanai EMA, of pre-ostoeblasts suspended in 0.3 N saline with cell parameters from [16], and in the frequency range of 10 – 200 MHz. (A) The real and (B) imaginary part of permittivity for different cell concentrations.

The well established Debye theory predicts the CP spectra for numerous standard liquids to be:

$$\varepsilon^* = \varepsilon_\infty + \frac{\varepsilon_s - \varepsilon_\infty}{1 + j\omega\tau}, \tag{6.4}$$

where ε_s and ε_∞ are the constant permittivities at DC and optic frequencies respectively, and τ is the relaxation time constant.

The Debye theory assumes that the relaxation process of the polarization vector occurs exponentially. Here we use the Debye theory to validate system performance when applied to standard liquids with high ionic content such as saline solutions.

6.4 System Instrumentation

The CPM sensor used was a commercial open-ended coaxial probe (Agilent 8507D). Such sensors can be readily constructed as presented in [22], however, it was found that precise manufacture of small probe aperture dimensions, needed for our application, was difficult. The Agilent probe had an electrical opening smaller than the thickness of the sample and less than half the sample's surface area (inner radius: a = 0.33 mm, outer radius: b = 1.5 mm); it was terminated by a grounded conductive flange whose diameter was significantly greater than the sample (radius of 9.5 mm). These small probe dimension ratios facilitate modeling the probe's aperture fields [23].

Open-ended coaxial probes function in conjunction with material analyzers. An impedance analyzer (Agilent E4991A) was used because it implements an RF I-V measurement method which is considered to have better sensitivity than the reflection coefficient measurement produced by a network analyzer [24]. A computer was interfaced with the material analyzer through a GPIB (National Instruments) card for control and online data acquisition.

All measurements were performed under sterile conditions. The probe apparatus, less the impedance analyzer, with the aperture face up, was set under a laminar flow hood and fixed in position to avoid disturbance during measurement. A sample holder was made by cutting a 50 ml Falcon tube (Corning) and

attaching it to the top of the probe through a well fitted rubber o-ring. The complete system setup is illustrated in Fig. 6.2.

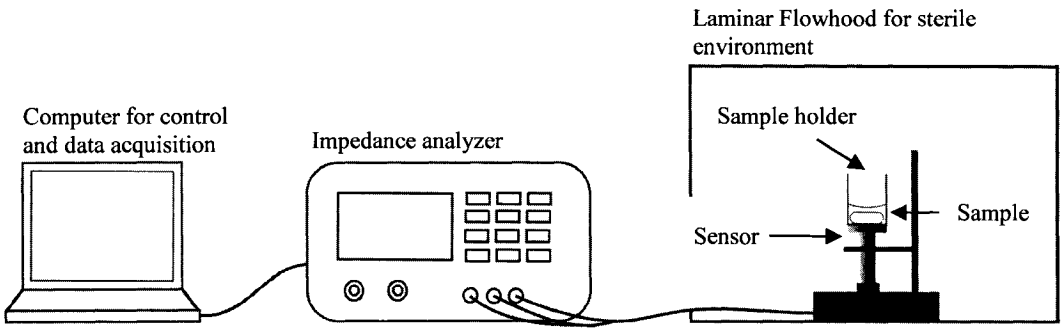

Figure 6.2. Experimental setup

6.5 Modeling

6.5.1 Reflection Model

The probe and impedance analyzer measure the impedance, admittance, and reflection coefficient of the sample. To extract the CPM the aperture admittance (Y_L) must be determined. This was done using the quasi-static model presented in [25]:

$$Y_L = \frac{j2\omega\varepsilon_0\varepsilon^*}{\left[\ln\left(b/a\right)\right]^2}\left\{I_1 - \frac{k^2 I_2}{2}\right\} + \frac{k^3\pi\omega\varepsilon_0\varepsilon^*}{12}\left[\frac{b^2-a^2}{\ln\left(b/a\right)}\right]^2 \quad \text{(S)} \tag{6.5}$$

where

$$k = \omega\sqrt{\varepsilon^*\varepsilon_0\mu_0} \tag{6.6}$$

$$I_1 = \int_a^b\int_a^b\int_0^\pi \frac{\cos(\phi)}{\sqrt{r^2+r'^2-2rr'\cos(\phi)}}\,d\phi\,dr\,dr' \tag{6.7}$$

$$I_2 = \int_a^b\int_a^b\int_0^\pi \cos(\phi)\sqrt{r^2+r'^2-2rr'\cos(\phi)}\,d\phi\,dr\,dr' \tag{6.8}$$

Where k is the wavenumber in the material medium, ϵ_0 and μ_0 are the permittivity and permeability of free space. Note that, a cylindrical coordinate system (r,ϕ,z) is used where primed coordinates represent the source points while unprimed ones represent the field points. The model requires only a single computation of its integrals per probe geometry allowing fast online performance. Furthermore,

isolating the sample permittivity is simplified when: the probe has a small electrical opening, and the sample has a high modulus of CP, such as biological tissue. When these conditions are met only the first term of (6.5) is necessary to model the aperture admittance of the probe [26], therefore:

$$\varepsilon^* = -j\frac{Y_L\left[\ln\left(b/a\right)\right]^2}{2\omega\varepsilon_0 I_1}. \tag{6.9}$$

The inherent length of the probe, the physical imperfections of the system and deviations from assumptions result in certain errors in the reflection coefficient measurement. These imperfections are corrected for by a calibration procedure based on a linear two-port network with a scattering matrix S as presented in Fig. 6.3 [27].

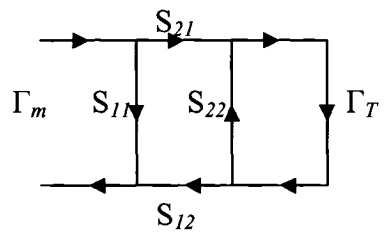

Figure 6.3. 2-port scattering network

The network relates the measured reflection coefficient to the true reflection coefficient:

$$\Gamma_T = \frac{\Gamma_m - S_{11}}{\Gamma_m S_{22} - \left(S_{11}S_{22} - S_{21}S_{12}\right)}, \tag{6.10}$$

where Γ_m and Γ_T are respectively the measured and true reflection coefficients.

Consequently, to evaluate the three unknowns (S_{11}, S_{22}, $S_{21}S_{12}$), three calibration standards with known dielectric behavior are required. The standards we used were: air ($\Gamma_1 = 1$), a short circuit, ($\Gamma_2 = -1$), and water (Γ_w) whose CP was determined using the Debye equation with parameter values from [26,28]. The admittance was then calculated from (6.5) and mapped to the reflection coefficient:

$$\Gamma_w = \frac{1-Y_w}{1+Y_w} \tag{6.11}$$

where Y_w and Γ_w are, respectively, the admittance and reflection coefficient of water. The network parameters where then solved:

$$S_{11} = \frac{\Gamma_{m3}(\Gamma_{m2}-\Gamma_{m1}) - \Gamma_w\Gamma_{m1}(\Gamma_{m2}-\Gamma_{m3}) + \Gamma_w\Gamma_{m2}(\Gamma_{m3}-\Gamma_{m1})}{-(\Gamma_{m1}-\Gamma_{m2}) - \Gamma_w(\Gamma_{m2}-\Gamma_{m3}) + \Gamma_w(\Gamma_{m3}-\Gamma_{m1})}, \tag{6.12}$$

$$S_{22} = \frac{\Gamma_w(S_{11}-\Gamma_{m2}) - (\Gamma_{m3}-S_{11})}{\Gamma_w(\Gamma_{m2}-\Gamma_{m3})}, \tag{6.13}$$

$$S_{12}S_{21} = (S_{11}-\Gamma_{m2})(1+S_{22}). \tag{6.14}$$

Where, Γ_{m1}, Γ_{m2}, and Γ_{m3} are, respectively, the reflection coefficients of the measured standards: air, short circuit and water.

The validity of this model was tested using standard liquids having well-described CP Debye curves: 100 % ethanol, 100 % methanol, 0.1 N saline solution, and 0.3 N saline solution. The accuracy of the model was evaluated by calculating the percentage variance accounted for (VAF), defined as the square of the correlation coefficient r^2, between the measured and theoretical CP.

Table 6.1 summarizes the VAF analysis between the measured and Debye CP of the standards. The model performed best for the real CP of liquids with low ionic content such as ethanol and methanol. However, the imaginary CP of the low ionic liquids was less accurate, especially that of methanol. Both methanol and ethanol have a small $|\varepsilon^*|$ for low frequencies as opposed to the saline and cell medium solutions. CP measurements of liquids with a small $|\varepsilon^*|$, performed with a small aperture probe, yield greater uncertainties than for liquids with large $|\varepsilon^*|$ [26]. However, in this case there was large error when calculating the real part of saline solutions at low frequencies. Fig 6.4A shows that the measured real CP of 0.3 N saline deviated increasingly from the Debye curve with decreasing frequency. In contrast, the loss factor measurement, shown in Fig 6.4B, remained accurate even at low frequencies.

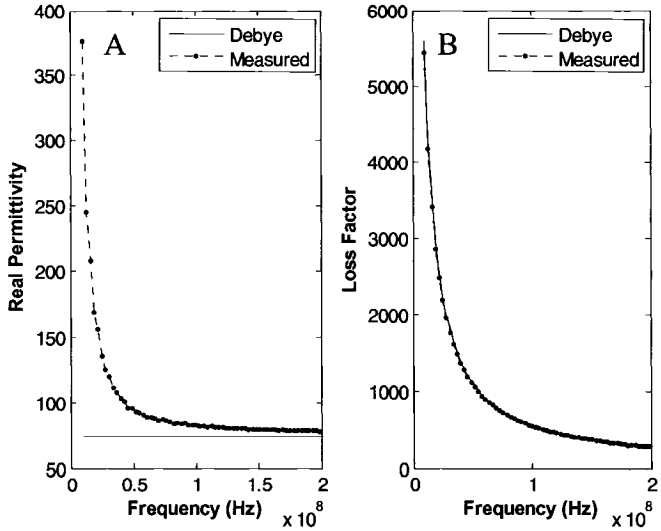

Figure 6.4. CP spectrum of (0.3 N) saline as measured and calculated by the Debye equation: (A) real part (VAF = 52.32 %), (B) imaginary part (VAF = 99.93 %).

The models from [29] and [30] were implemented to verify that the observed phenomenon was not specific to the chosen aperture admittance model; however, their CPM calculation showed similar errors. Thus, the error was not model specific but exhibited the traits of polarization phenomena that become more prevalent at low frequencies, specifically for electrolyte solutions, and corrupts the real part of CPM. Electrode polarization is expected to occur at frequencies below 10 MHz, in the current case the observed polarization phenomena commences at approximately 200 MHz. Similar CPM behavior for saline spectrums was depicted graphically in [31] but not commented on.

Table 6.1. VAF as a measure of fit between the CPM of different standard liquids and their corresponding Debye curves

	VAF (%)	
	Real	Im.
Ethanol	99.99	93.30
Methanol	99.99	76.26
Saline 0.1 N	95.49	99.85
Saline 0.3 N	52.32	99.94

Validation of measurements from cell suspensions, and seeded scaffolds is difficult because there is little data on the CP spectra of cell mediums. However, it has been noted that saline solutions generally have similar CP spectrums with slight offsets. Therefore, it is assumed that if the real CPM of saline is in error that of the cell medium will be too. As described below, the problem is addressed by modifying the EMA so that it is a function of the loss factor only.

6.5.2 Effective Medium Approximation

The Hanai function, as derived by Boyle, was implemented to model a cell-polymer matrix immersed in cell medium. The function allows for different cell morphologies and is applicable to high volume fractions:

$$(1-\varphi)=\left(\frac{\varepsilon^*_{eff}(\omega)-\varepsilon^*_{cell}(\omega)}{\varepsilon^*_{m}(\omega)-\varepsilon^*_{cell}(\omega)}\right)\left(\frac{\varepsilon^*_{m}(\omega)}{\varepsilon^*_{eff}(\omega)}\right)^{n} \tag{6.15}$$

Where the parameter n determines the morphology of the inclusions: for lamellar n = 1, for cylindrical n = 1/2, and for spherical n = 1/3. The effective CP is the CPM of the cell polymer matrix immersed in α-MEM; the medium CP is the CPM of an empty scaffold, the control, immersed in medium; the cell CP and volume fraction are the elements that must be solved for from the empirical data. Our application focuses on a lamellar cell morphology since attached pre-osteoblasts are innately lamellar. Consequently, the formulation can be rewritten as:

$$\varepsilon^*_{eff}=\frac{\varepsilon^*_{m}\varepsilon^*_{cell}}{(1-\varphi)\varepsilon^*_{cell}+\varphi\varepsilon^*_{m}}. \tag{6.16}$$

The cell is modeled as a lamellar cell with a plasma membrane of fixed thickness enveloping a uniform cytoplasm of CP (ϵ^*_{cyt}). The cell volume is related to the EMA through the parameter v which assumes a spherical cell shape irrespective of n. The CP of a cell is then defined as:

$$\varepsilon^*_{cell}=\frac{\varepsilon'_{mem}\varepsilon^*_{cyt}}{(1-v^3)\varepsilon^*_{cyt}+v^3\varepsilon'_{mem}}. \tag{6.17}$$

Where ϵ'_{mem} is the real CP of the cell membrane, ε^*_{cyt} is the complex permittivity of the cytoplasm and v = 1-(d/r_c), where r_c is the cell radius and d is the thickness of the membrane.

This expression for the effective CP can be separated into its real and imaginary components:

$$\mathrm{Re}\left[\varepsilon^*_{eff}(\omega)\right]=\frac{(\varepsilon'_m\varepsilon'_{cell}-\varepsilon''_m\varepsilon''_{cell})\left[(1-\varphi)\varepsilon'_{cell}+\varphi\varepsilon'_m\right]+(\varepsilon'_{cell}\varepsilon''_m+\varepsilon''_{cell}\varepsilon'_m)\left[(1-\varphi)\varepsilon''_{cell}+\varphi\varepsilon''_m\right]}{\left[(1-\varphi)\varepsilon'_{cell}+\varphi\varepsilon'_m\right]^2+\left[(1-\varphi)\varepsilon''_{cell}+\varphi\varepsilon''_m\right]^2} \tag{6.18}$$

$$\mathrm{Im}\left[\varepsilon^*_{eff}(\omega)\right]=\frac{(\varepsilon'_{cell}\varepsilon''_m+\varepsilon''_{cell}\varepsilon'_m)\left[(1-\varphi)\varepsilon'_{cell}+\varphi\varepsilon'_m\right]-(\varepsilon'_m\varepsilon'_{cell}-\varepsilon''_m\varepsilon''_{cell})\left[(1-\varphi)\varepsilon''_{cell}+\varphi\varepsilon''_m\right]}{\left[(1-\varphi)\varepsilon'_{cell}+\varphi\varepsilon'_m\right]^2+\left[(1-\varphi)\varepsilon''_{cell}+\varphi\varepsilon''_m\right]^2}. \tag{6.19}$$

From (6.18) and (6.19) it is evident that the cell volume fraction can be extracted from either the real or imaginary part of the effective CPM. However, the real part of the effective CP is largely a function of the real CP of α-MEM's which are corrupted and therefore can be expected to be in error. The effective loss factor is also a function of the real part of the CPM of α-MEM's but it plays a minor role, i.e., if $\varepsilon''^2_m, \varepsilon''^2_{cell} >> \varepsilon'^2_m$ then (6.19) can be closely approximated by:

$$\mathrm{Im}\left[\varepsilon^*_{eff}(\omega)\right]=\frac{(1-\varphi)(\varepsilon'^2_{cell}\varepsilon''_m+\varepsilon''_m\varepsilon''^2_{cell})+\varphi(\varepsilon''^2_m\varepsilon''_{cell})}{((1-\varphi)\varepsilon'_{cell})^2+[(1-\varphi)\varepsilon''_{cell}+\varphi\varepsilon''_m]^2}. \tag{6.20}$$

The accuracy of the approximation was evaluated by the normalized error defined as:

$$E_n=\frac{|x-\bar{x}|}{x}, \tag{6.21}$$

where, x and $\bar{x}$ are, respectively, the results of the true and approximate formulations.

Fig. 6.5 shows the plot of the normalized error for volume fractions over 10 - 200 MHz. For a cell volume fraction less than 0.3 the error due to the approximation is less than 1 % and decreases further for smaller volume fractions. The cell volume fractions used here are at most 100 hundred times smaller that the 0.3 limit. In our previous research and those of other groups [32] using similar scaffolds the cell volume fraction was never greater than 0.03. Consequently, the use of the approximation results in minimal loss to the accuracy of the EMA.

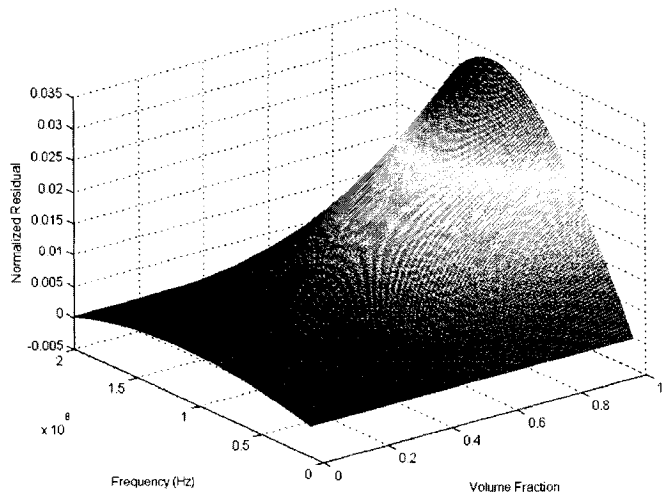

Figure 6.5. Normalized error due to EMA approximation, i.e. the normalized error between the imaginary Hanai formulation (6.19) and the proposed approximation (6.20) where the host medium is 0.3 N saline as per (6.4) and the cell parameters are from [16].

Cell parameters were retrieved by fitting (6.20) to the measured effective permittivity. A complex non-linear fitting procedure implementing the trust region reflective-Newton algorithm (Matlab optimization toolbox) was used to fit the imaginary part of the complex permittivity. The mean and standard deviation of previously published cell parameters [13-15] for seeded pre-osteoblasts were used, respectively, as the seed values and trust regions for the applied fitting algorithm. To determine the quality of fit the VAF between the effective and modeled permittivity and normalized residuals were calculated and analyzed. All mathematical modeling and algorithm implementation was performed in Matlab (The MathWorks).

6.6 Cell Polymer Sample Preparation

6.6.1 Micro-porous Scaffold

Micro-porous polymer scaffolds were made from high molecular weight chitosan (Sigma Aldrich) – a polysaccharide that is a partially deacytalated derivative of chitin. Chitosan has been used often for bone tissue engineering

because it supports Osteoblast and Chondrocyte survival and phenotypic expression [20, 21].

Scaffolds were prepared by dissolving the chitosan at a 2% concentration in a water acetic acid mixture (1% v/v). The resulting gel was pressure filtered into flasks to remove non-dissolved chitosan. The flasks where sonicated for one hour to remove air bubbles. Then, the gel was cast in 24 well plates (Corning, U.S.A) and frozen at -20 °C over night within Styrofoam boxes to slow freezing and generate the desired pore size [20]. Once frozen, the gels where lyophilized over a period of three days. Subsequently, each scaffold was carefully trimmed to yield two cylindrical samples approximately 3 mm high, with uniform top and bottom surfaces, and a diameter of 15 mm. Flat sample surfaces are imperative to ensure repeatability. Scaffolds from each batch were randomly selected for porosity measurements. Porosity was calculated to be 94.3 ± 2 % by the CPM method as previously described and validated in [15].

Scaffolds were then immersed in progressively lower concentrations of ethanol – from 100 % to 70 % over a 48 hour period to neutralize and sterilize the sample [20]. The scaffolds were then stabilized in a phosphate-buffered saline (PBS) solution with pH 7.2. Three hours before seeding, the scaffolds were washed in alpha minimum essential medium (α-MEM) to remove any traces of PBS and incubated to match the environment of the cell culture. Prior to seeding the medium was removed from the scaffolds.

6.6.2 Cell Seeding

The Pre-osteoblast MC3T3-E1 subclone 14 (ATCC, USA) cell line was used as the cell model because it forms well mineralized ECM after 10 days when stimulated with differentiation medium and has been shown to attach well to porous structures [15]. The cells were cultivated in α-MEM with L-glutamine and sodium bicarbonate at 2.5 g/L, supplemented with 10% foetal bovine serum and 1% penicillin streptomycin (Biomedia, Canada).

Each scaffold was seeded with 1 ml of solution having a cell concentration prepared by means of a hemacytometer (Hausser Scientific). The solution was

carefully injected into the sponge-like scaffold through a micro-pipette tip. The resulting cell-polymer matrix was incubated at 37°C in an atmosphere of 100% humidity and 5% CO_2. The medium was changed daily when a measurement was performed.

6.7 Experiments

CPM was performed at room temperature over a frequency range of 10 - 200 MHz with a sampling interval of 20 kHz. Each sample was gently centered atop the probe and three CPMs were performed and averaged. The probe was calibrated prior to each set of measurements.

6.7.1 Cell Concentration Variation

First, the system's functionality was tested by taking CPMs of scaffolds with incrementally greater concentrations of cells to emulate cell proliferation. Tissue growth evaluation entails two CPMs: the effective CPM and the CPM of the medium (the control measurement). Two methods of performing the control measurement were explored. In the first, measurements of the scaffold were taken prior to seeding and used as the control for all further measurements. In the second, a separate control scaffold was used that remained unseeded throughout the experiment but underwent the same treatment. Ideally, the control scaffold should be cut from the same original cylindrical cast as the sample and so have a similar structure.

CPM of thirty paired seedless scaffolds, from the same cast, immersed in α-MEM were taken at room temperature as control measurements. The pairs were then separated into two sets: seeded and corresponding controls. The seeded set was further divided into five sets, seeded with 1 ml of 0.2 0.4, 0.45, 0.5, or 0.6 × 10^6 cells/ml suspensions. The cell-polymer matrices were then incubated for six hours along with the controls. Prior to measurement, samples were allowed to cool to room temperature. For every CPM of a cell-polymer matrix, a

corresponding control CPM was performed to evaluate the two methods of control measurement.

In previous work, we found that the calculated cell concentrations overestimated the true values but the relative measurements were generally correct. The overestimate was likely due to greater conglomeration of cells on the scaffold side of seeding which also acts as the bio-interface of the probe. In the current experiments a calibration measurement, which is used as a scaling factor, was performed to map the cell concentration measurement to a realistic cell number (N_{cells}). The set of scaffolds seeded with 0.2×10^6 cells was used for the calibration:

$$N_{cells} = \phi_{meas} \times \frac{N_{cal}}{\phi_{cal}}, \tag{6.21}$$

where N_{cal} is the number of cells seeded onto the calibration scaffold, ϕ_{cal} is the average calculated cell volume fraction of the calibration set, and ϕ_{meas} is the measurement to be mapped to a cell number.

Fig. 6.6A shows a typical loss factor spectrum measurement from 10 – 200 MHz of a seeded scaffold with the corresponding fit and control measurement. Seeded scaffolds had a lower effective loss factor which is highlighted by the insert. The decrease in the loss factor is attributed to the low conducting cell membrane and followed the expected theoretical behavior presented in Fig 6.2B.

The proposed EMA formulation produced excellent data fits with an average VAF greater than 99 %. In addition, the average normalized residuals, as shown in Fig. 6.6B, were insignificant with maximum amplitude of 0.4 %, and a minimal trend with an offset. The observed non-white nature of the residuals was attributed to the EMA's imperfect model of the sample (i.e. the potentially uneven cell distribution within the sample, the varied cell morphology, and the simplified cell model).

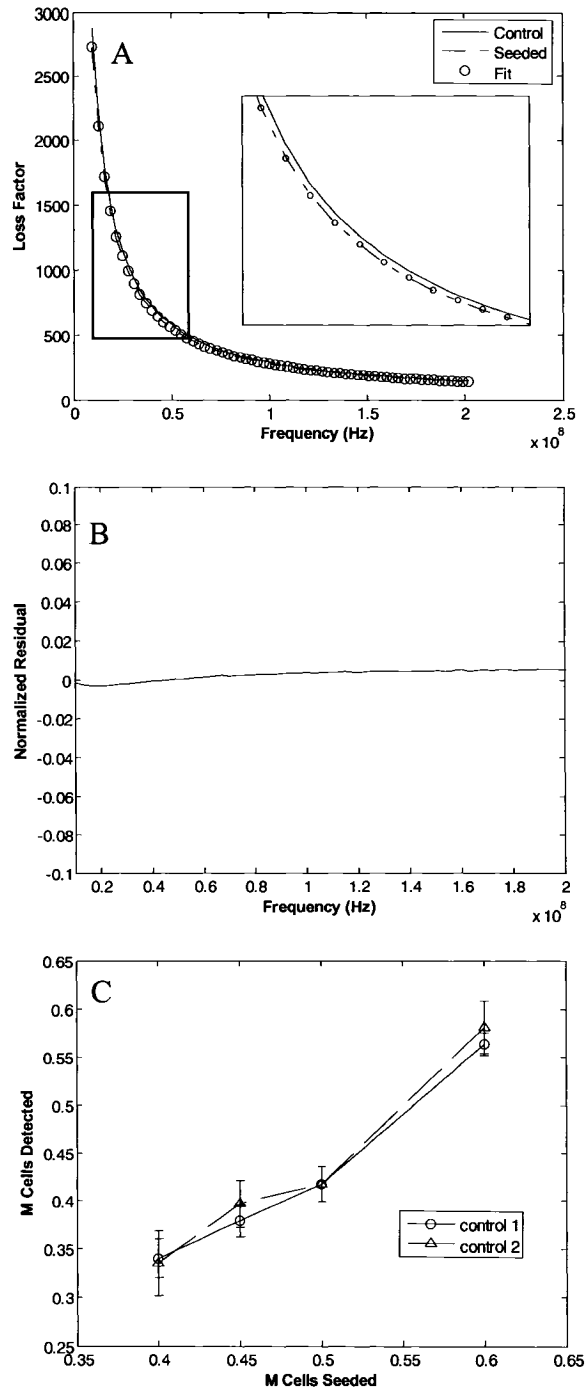

Figure 6.6. Representative data for the loss factor measurement and fit: (A) loss factor of seeded and seedless scaffold and corresponding fit (VAF = 99.99 %), (B) the average normalized residuals, (C) calculated cell number for the four sets of scaffolds for the two control methods: control 1 is a CPM of the scaffold prior to seeding, control 2 is a CPM of a seedless scaffold cut from the same cast as the sample. An analysis of variance (ANOVA) of each control group showed them both to be statistically different ($p<0.0001$). However, note that the standard error bars of control method 2 overlap for cell populations differing by 0.05×10^6 cells.

Fig. 6.6C shows the cell numbers estimated after calibration with both types of control methods. According to hemacytometer readings the relative cell count in both cases is an underestimate of the seeded numbers; it is unlikely that all the cells adhered to the scaffolds. The general progressive increase of concentration between the sets was recorded. The nonlinearity of the trend was likely due to disproportionate cell adhesion, between the experiment's sets, to the polymer scaffold. A statistical difference was recorded between sets of scaffolds differing by 0.1×10^6 cells for both control methods. Using the same scaffold prior to seeding as control measurement permitted greater statistical discrimination between scaffolds seeded with cell numbers differing by 0.05×10^6 cells. However, the resolution was far worse using an independent scaffold as a control; it increased the measurement error and reduced the resolution of the system as depicted by the overlapping standard error bars. Although, there is no accurate way to validate the absolute cell numbers in the scaffolds, the cell numbers presented in Fig 6.6C as per the calibration equation (6.21) are in good accordance with our expectation. The detected cell numbers are expected to underscore the number of seeded cells which should be the case since it is expected that not all cells will attach themselves to the scaffold.

It is assumed that all the differences between the control and the seeded samples are due to the presence of cells; thus, structural irregularities between the control and sample will bias the cell concentration measurement. However, the independent control method is more flexible because it allows system calibration between measurements since the control CPM can be redone each time – an important aspect for prolonged experiments.

The cell parameters estimated by the system are presented in Table 6.2. Their values constitute the cell signature and volume fraction of the particular cell line used and correspond to typical values for generic cells. It has been previously shown [14,15] that different cell lines have particular cell signatures. Observing the change of the cell signature over time might prove to be useful to recognize the differentiation of a stem cell.

Table 6.2. The cell signature and cell concentration as retrieved by the system during the study of cell concentration variation

Seeded Cells (M)	ϵ'_{mem}		ϵ'_{cyt}	
	Mean	Std dev	Mean	Std dev
0.4	33.54	18.41	80.13	7.14
0.45	28.81	15.77	79.11	6.27
0.5	30.89	16.92	80.25	5.91
0.6	26.68	15.34	77.68	5.72

Seeded Cells (M)	σ_{cyt}		ϕ	
	Mean	Std dev	Mean	Std dev
0.4	0.1929	0.0189	0.0741	0.0075
0.45	0.1960	0.0164	0.0825	0.0064
0.5	0.1779	0.0357	0.0909	0.0071
0.6	0.1749	0.0380	0.1225	0.0045

6.7.2 Cell Proliferation

To produce a standard curve for cell proliferation within micro-porous polymer scaffolds, fifty-six scaffolds were seeded with 0.5×10^6 cells and observed over a period of two weeks. Four cell-polymer matrices were measured daily, after which four scaffolds were sacrificed for use in other validation techniques. The length of the experiment required numerous equipment calibrations. Consequently, the control CPM used was from a non-seeded scaffold from the same cast as the sample performed before each proliferation measurement – such as control 2 from the cell concentration variation experiment.

Proliferation trends were validated with a DNA concentration assay (CyQuant) of three samples per day of experiment. Scaffolds for the DNA assay where gently washed in PBS, to remove traces of α-MEM, frozen at -80 °C until all samples were collected. They were then brought back to room temperature in lyses buffer and the DNA concentration assay was performed and the relative fluorescence measurement trends were compared to the relative cell concentrations extracted from CPM. Scanning electron microscopy (SEM) was performed on a scaffold from each measurement day to confirm cell presence, morphology, and scaffold structure.

Fig. 6.7A shows the CPM cell concentration estimates for scaffolds monitored over a period of two weeks. There was an apparent decrease in concentration over the first four days of the experiment; this is consistent with the DNA assay curve shown per Fig. 6.7B. Cell proliferation was observed to begin after day 4; whereupon, the cell concentration increased and then plateaued with sporadic concentration variance after day 8. The trend in the data was not smooth, during each measurement and medium change there is chance of cell detachment and/or cell death. Nonetheless, the CPM and DNA cell proliferation curves indicate a general increase in the cell concentration within the scaffolds over the 14 day experiment period.

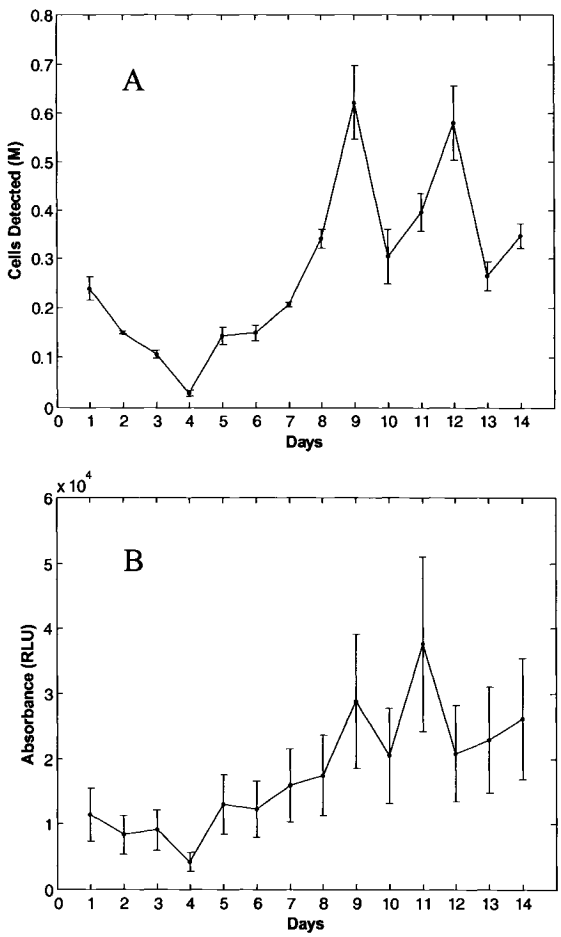

Figure 6.7. Proliferation study of scaffolds seeded with 0.5×10^6 pre-osteoblasts over a period of 14 days. (A) Relative cell count as extracted by the CPM method when applied to 4 scaffolds a day, (B) Fluorescence DNA concentration assay applied to 3 scaffolds a day.

Table 6.3 reports that the estimated average cell signature of the proliferation study was within the range presented in Table 6.2 and did not vary significantly with the change of volume fraction.

Table 6.3. The average cell signature retrieved over the 14 day proliferation study

ϵ'_{mem}		ϵ'_{cyt}		σ_{cyt}	
Mean	Std dev	Mean	Std dev	Mean	Std dev
31.80	19.72	79.18	7.28	0.1929	0.0189

The large error bars of the DNA assay data are likely due to the difficulty of proportionally removing the cells from the scaffold. DNA assays used for scaffolds were designed for two-dimensional cell culture and therefore there is no good protocol to remove cells from the scaffold and count them or their parameters. Consequently, it has been reported that it is difficult to deduce meaningful results from assays performed on three-dimensional cultures [31], i.e., the results should be treated as an estimate of the relative trend of the cell proliferation. Therefore, the only significant trends of Fig 6.7B are the decrease of cell concentration on day 4 of the experiment followed by a general increase in cell concentration over the next 8 days. These trends correspond to the CPM cell proliferation curve of Fig. 6.7A. As well, these data correspond well to our previous results [15]. Furthermore, the similar trend of increased cell proliferation over the first two weeks of incubation has been reported by other authors [32]. Of note is that we are not aware of reports of cell proliferation measured at a daily frequency, with such a number of cells. This is likely due to the large work load associated with such measurements and highlights the potential of the CPM system.

Fig. 6.8 presents the SEM analysis; there is good cell adherence to the scaffold. Specifically, Fig. 6.8A shows that the cells are attached evenly across the scaffold's surfaces and are migrating well into the inclusions. The scaffolds exhibited interconnected pore morphology and a pore size of 100 - 300 μm, which corresponds well to values reported by other groups producing polymer scaffolds

[33]. The general cell morphology was lamellar with some small fibrillar elements elongated across pores as shown in Fig. 6.8B. This supports our assumptions that the cell shape is lamellar for the EMA.

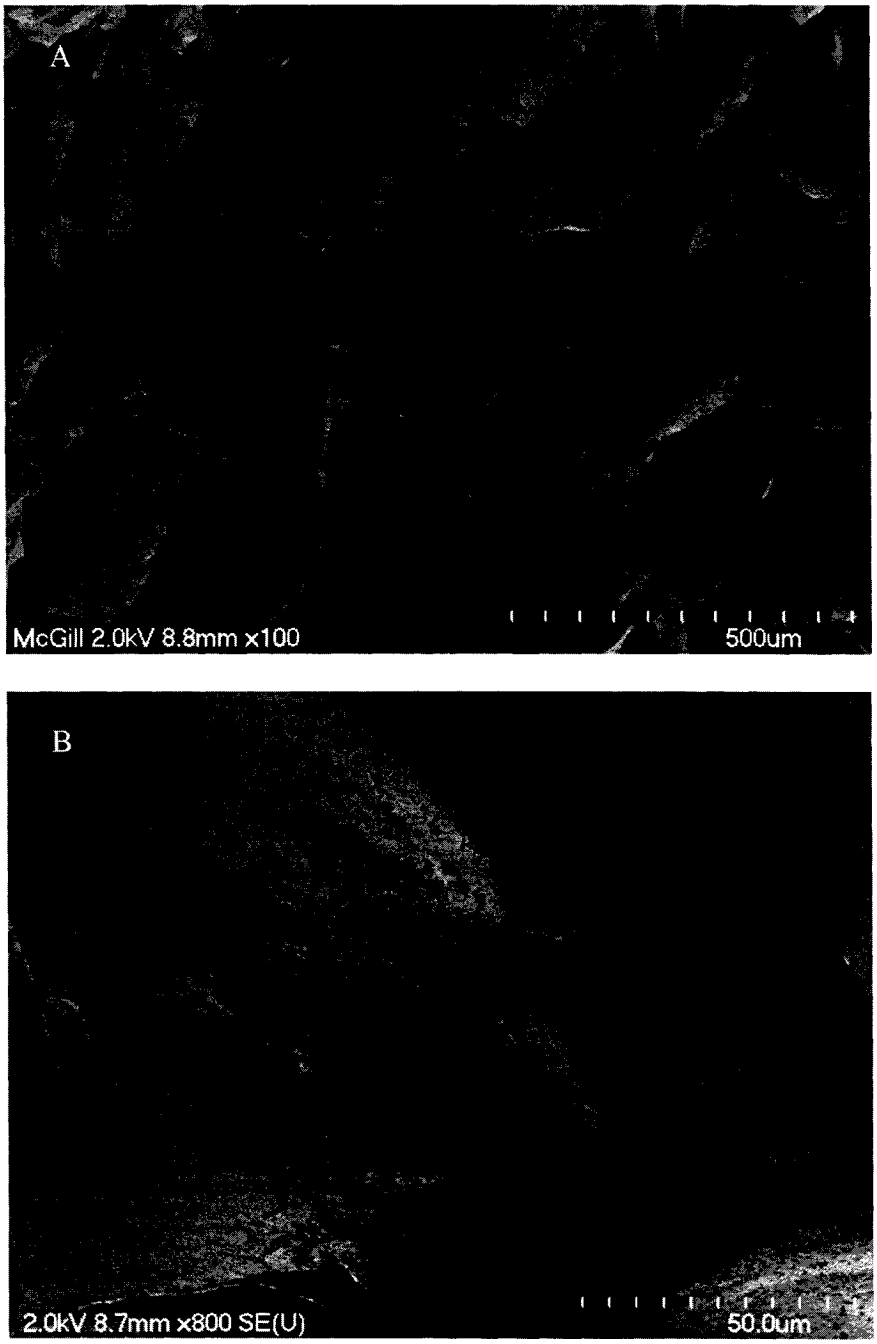

Figure 6.8. SEM of a scaffold on the 9th day of incubation during the proliferation study. (A) The scaffold surface interfaced with the probe, and (B) a magnification view of a single pre-osteoblast cell attached to the same scaffold.

6.8 Concluding Remarks

A system for tissue engineering application was built to non-destructively assess cell proliferation within micro-porous polymer scaffolds. Based on the CPM, the system comprises five elements: (i) the bio-interface, a micro-porous chitosan scaffold seeded with pre-osteoblasts, (ii) the biosensor, an open-ended coaxial probe (iii) an impedance analyzer the reflection coefficient of the sample, (iv) a quasi-static mathematical model of the probe's aperture admittance which related the measured reflection coefficient to the CP of the sample, (v) Hanai EMA used to extract cell concentration and signature from the CPM.

We have demonstrated that the Hanai EMA for lamellar cell morphology can be approximated as a function of the loss factor of the CPM with minimal error. This approximation eliminates the corruption of the real part of CPM which becomes prevalent at low frequencies where the CPM is most sensitive to cell concentration.

The system successfully discriminated scaffolds seeded with different pre-osteoblast cell concentrations as shown by Fig. 6.6C of the cell concentration variation experiment. The CPM reported increased cell numbers for the progressively greater cell dense scaffolds that were in good proximity to the seeded values but did not increase linearly possibly because of uneven cell attachment between the scaffold sets. Cell concentration measurements where shown to be more precise when the control measurement was the scaffold prior to seeding (control 1) versus another empty scaffold from the same cast (control 2).

The cell proliferation experiment demonstrated the potential of the system by producing a standard data for cell proliferation monitoring by 56 scaffolds over a period 14 days. The calculated relative cell concentration changes were similar to the fluorescence data produced by the concurrent DNA assay and to previously reported cell proliferation trends. In addition, the system returned the same cell signature, irrespective of cell volume, from each set of measurements in both experiments. Cell signature measurements could be useful for cell line recognition and observing stem cell differentiation.

Current studies are exploring the effects of ECM on the kinetics of the cell concentration data. As well, there is focus on modifying the system to map the cell distribution within the scaffold. We believe that the CPM system will evolve into a useful tool for monitoring stem cell differentiation and proliferation in micro-porous polymer scaffolds.

6.9 Acknowledgments

This study was financially supported by the Fonds Quebecois de la Recherche sur la Nature et les Technologies (FQRNT) and the Natural Sciences and Engineering Research Council (NSERC).

Agilent Technologies are greatly appreciated for their consultation and equipment loan. In addition, the authors would like to thank Dr. Teodor Veres from IMI-NRC for his consultation, Line Mongeon for SEM analyses, and Jean-Philippe St-Pierre for guidance with cell-culture and DNA assay protocols.

6.10 References

[1] L. G. Griffith, and G. Naughton, " Tissue Engineering-Current Challenges and Expanding Opportunities," Science, vol. 295, pp. 1009-1016, 2002.

[2] P. Bianco, and P. G. Robey, " Stem Cells in Tissue Engineering," Nature, vol. 414, pp. 118-121, 2001.

[3] M. Sittinger, D. W. Hutmacher, and M. V. Risbud, "Current Strategies for Cell Delivery in Cartilage and Bone Regeneration," Current Opinion in Biotechnology, vol. 15, pp. 411-418, 2004.

[4] J. J. Marler, J. Upton, R. Langer, and J. P.Vacanti, "Transplantation of Cells in Matrices for Tissue Regeneration," Advanced Drug Delivery Reviews, vol. 33, pp. 165-182, 1998.

[5] D. W. Hutmacher, "Scaffolds in Tissue Engineering Bone and Cartilage," Biomaterials, vol. 21, pp. 2529-2543, 2000.

[6] P. Ducommun, A. Kadouri, U. von Stockar, and I. W. Marison, "On-line Monitoring of Animal cell Concentration in Two Industrial High-Density

Culture Processes by Dielectric Spectroscopy," Biotechnology and Bioengineering, vol. 77, pp. 316-317, 2002.

[7] L. Olsson and J. Nielsen, "On-line and *In situ* Monitoring of Biomass in Submerged Cultivations," Trends in Biotechnology, vol. 15, pp. 517-522, 1997.

[8] G. Locher, B. Sonnleitner, and A. Fiechter, "On-line Measurement in Biotechnology: Techniques," Journal of Biotechnology, vol. 25, pp. 23-53, 1992.

[9] K. Asami, "Characterization of Biological Cells by Dielectric Spectroscopy," Journal of Non-Crystalline Solids, vol. 305(1-3), pp. 268-277, 2002.

[10] G. H. Markx, and C. L. Davey, " The Dielectric Properties of Biological Cells at Radiofrequencies: Applications in Biotechnology," Enzyme and Microbial Technology, vol. 25(3-5), pp. 161-171, 1999.

[11] R. Pethig, and D. B. Kell, "The Passive Electrical Properties of Biological Systems: their Significance in Physiology, Biophysics and Biotechnology," Physics in Medicine and Biology, vol. 32, no. 8, pp. 933-970, 1987.

[12] J. P. Grant, R. N. Clarke, G. T. Symm, and N. M. Spyrou, "A Critical Study of the Open-Ended Coaxial Line Sensor Technique for RF and Microwave Complex Permittivity Measurements," Journal of Physics E: Scientific Instruments, vol. 22, pp. 757-770, 1989.

[13] C. L. Pournaropoulos, and D. K. Misra, "The Co-axial Aperture Electromagnetic Sensor and its Application in Material Characterization," Measurement Science and Technology, vol. 8, pp. 1191-1202, 1997.

[14] P. O. Bagnaninchi, M. Dikeakos, T. Veres, and M. Tabrizian, "Monitoring of Stem Cell Proliferation and Differentiation using a Permittivity Responsive Biointerface," Materials Research Society Symposium Proceedings, vol. 773, pp. N7.12.1, 2003.

[15] P. O. Bagnaninchi, M. Dikeakos, T. Veres, and M. Tabrizian, "Towards On-Line Monitoring of Cell Growth in Microporous Scaffolds: Utilization and Interpretation of Complex Permittivity Measurements," Biotechnology and Bioengineering, vol. 84, pp. 343-350, 2003.

[16] P. O. Bagnaninchi, M. Dikeakos, T. Veres, and M. Tabrizian, "Complex Permittivity Measurement as a New Non-invasive Tool for Monitoring *In-vitro* Tissue Engineering and Cell Signature through the Detection of Cell

Proliferation, Differentiation , and Pre-tissue Formation," IEEE Transactions on NanoBioscience, vol. 3, pp. 243-250, 2004.

[17] C. L. Davey and D. B. Kell, "The Influence of Electrode Polarization on Dielectric Spectra, with Special Reference to Capacitive Biomass Measurements I. Quantifying the Effects on Electrode Polarization of Factors Likely to Occur During Fermentations," Bioelectrochemistry and Bioenergetics, vol. 46, pp. 91-103, 1998.

[18] F. Bordi, C. Cametti, and T. Gili, "Dielectric Spectroscopy of Erythrocyte Cell Suspensions. A Comparison between Looyenga and Maxwell-Wagner-Hanai Effective Medium Theory Formulations," Journal of Non-Crystalline Solids, vol. 305, pp. 278-284, 2002.

[19] P. Zoltowski, "On the Electrical Capacitance of Interfaces Exhibiting Constant Phase Element Behaviour," Journal of Electroanalytical Chemistry, vol. 443, pp. 149-154, 1998.

[20] A. Lahiji, A. Sohrabi, D. S. Hungerford, and C. G. Frondoza, "Chitosan Supports the Expression of Extracellular Matrix Proteins in Human Osteoblasts and Chondrocytes," Journal of Biomedical Material Research, vol. 51(4), pp. 586-595, 2000.

[21] S. V. Madihally, and H. W. T. Matthew, "Porous Chitosan Scaffolds for Tissue Engineering," Biomaterials, vol. 20, pp. 1133-1142, 1999.

[22] N. I. Sheen, and I. M. Woodhead, "An Open-Ended Coaxial Probe for Broad- Band Permittivity Measurement of Agricultural Products," Journal of Agricultural Engineering Research, vol. 74, pp. 193-202.

[23] D. D. Zutter, "Design Rules for an Experimental Setup using an Open-Ended Coaxial Probe Based on Theoretical Modeling," IEEE Transactions on Instrumentation and Measurement, vol. 43, 1994.

[24] "Agilent Technologies Impedance Measurement Handbook" Agilent Technologies, 2003.

[25] D. K. Misra, "A Quasi-Static Analysis of Open-Ended Coaxial Lines" IEEE Transactions on Microwave Theory and Techniques, vol. mtt-35, 1987.

[26] C. L. Pournaropoulos, "A Study on the Coaxial Aperture Electromagnetic Sensor and its Application in Material Characterization" PhD dissertation, The University of Wisconsin-Milwaukee, 1996.

[27] J. Fitzpatrick, "Error Models for Systems Measurement," Microwave Journal, pp. 63-66, 1978.

[28] J. Dinebeditto and A. Uhlir, Jr.,"Frequency Dependance of 50 Ω Coaxial Open-Circuit Reflection Standard," IEEE Transactions on Instrumentation and Measurement, vol. IM-30, pp. 228-229, 1981.

[29] D. V. Blackham and R. D. Pollard, "An Improved Technique for Permittivity Measurements Using a Coaxial Probe," IEEE Transactions on Instrumentation and Measurement , vol. 46, pp. 1093-1099, 1997.

[30] M. A. Stuchly, M. Brady, S. Stuchly, and G. Gadja, "Equivalent Circuit of an Open-Ended Coaxial Line in a Lossy Dielectric," IEEE Transactions on Instrumentation and Measurement, vol. 31, pp. 116-119, 1982.

[31] B. G. Colpitts, "Temperature Sensitivity of Coaxial Probe Complex Permittivity Measurements: Experimental Approach," IEEE Transactions on Microwave theory and Techniques, vol. 41, pp. 229-233

[32] K. W. Ng, D. T. Leong, and D. W. Hutmacher, "The Challenge to Measure Cell Proliferation in Two and Three dimensions," Tissue Engineering, vol. 11(1-2), pp. 182-91, 2005.

[33] S. L. Ishaug-Riley, G. M. Crane-Kruger, M. J. Yaszemski, and A. G. Mikos, "Three-Dimensional Culture of Rat Calvarial Osteoblasts in Porous Biodegradable Polymers," Biomaterials, vol. 19, pp. 1405-1412, 1998.

CHAPTER 7
General Summary and Conclusion

Micro-porous polymer scaffolds provide structural and biochemical support with a pre-defined architecture for *in vitro* tissue engineering. It is important to measure cell proliferation nondestructively within these scaffolds to monitor the cultivation environment and the stages of tissue growth.

Permittivity measurements of seeded scaffolds previously performed by Bagnaninchi *et al* [1-3] were hampered by the low frequency limitation of their system which limited the measurements of the β-dispersion characteristic of cells. Nonetheless, as a proof of principle it demonstrated the capacity of the permittivity measurements to assess cell constituent variation within scaffolds. The suggested research segue was to modify the system to allow for lower frequency, more responsive, cell proliferation measurement.

This thesis investigated the components of a permittivity measurement system for the assessment of tissue growth within micro-porous polymer scaffolds at frequencies from 10-200 MHz. The system summary is presented in point form below.

1. Bio-interface: Chitosan micro-porous polymer scaffold, chosen to be representative of the current biomaterials trend.
2. Probe: Open-ended coaxial probe (Agilent, 8507D), a non-destructive probe.
3. Material analyzer: Impedance analyzer (Agilent E4991A), chosen for its response over 10-200 MHz.
4. Aperture admittance model: Quasi static formulation as presented by Misra *et al.* The model was chosen for its on-line applicability and simplicity when solving the inverse problem at low frequencies for biological media.
5. Effective medium theory: The Boyle formulation of the Hanai function was designed for a lamellar morphology and remains accurate for

increasing cell concentrations. The Boyle formulation facilitates isolating of the loss factor to remove the system's dependence on real permittivity of measurement.

At best performance, the system discerned between scaffolds that differed by 0.05 million cells at seeding. To achieve such sensitivity the control ambient measurement had to be performed using measurement of the scaffold prior to seeding with the same system calibration. The system calibration could not be sustained for prolonged monitoring. Thus, prior to measuring each seeded scaffold a corresponding control measurement was performed on an empty scaffold. When recalibration was necessary the system could only discriminate between scaffolds that differed by 0.1 million cells at seeding

The standard cell proliferation data curve showed an increase of average cell concentration over 14 days. The general trend of cell proliferation was in good accordance with that from the cell proliferation DNA assay.

Our results demonstrate that the system described here can be used as an on-line nondestructive tool for discriminating between micro-porous polymer scaffolds seeded with different pre-osteoblast cell concentrations. When applied as a monitoring device for seeded-scaffolds over time, the system can record cell proliferation and recognize cell signature.

7.1 Suggestions for Future Work

The system presented in this thesis makes a number of assumptions that facilitate the analytical description of the bio-interface formed by the cell seeded scaffold and the open-ended coaxial probe. The development of a system that eliminates some of these assumptions would increase system accuracy and reveal more information about the sample. Furthermore, the current experimentation of the CPM system was limited to one type of scaffold and two distinct cell lines. To best characterize system performance and application, measurement of various cell-scaffold composites should be explored under various conditions. The

following subsections discuss the avenues of future research for the development of a robust measurement system for tissue growth in scaffolds.

7.1.1 Scaffold Cell Distribution

A major assumption of the current system is that the vertical distribution of cells across the scaffold is constant. Hutmacher *et al* reported that when scaffolds are seeded the cells tend to remain on the scaffold side of seeding [4] as illustrated by Fig 7.1.

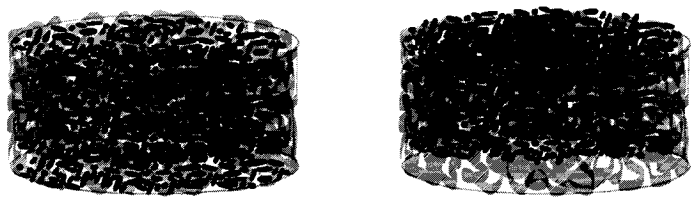

Assumed cell distribution Realistic cell distribution

Figure 7.1. Scaffold cell distributions

Uniform horizontal cell distribution is also assumed in this work; however, this assumption is relatively valid as can be seen by the scanning micrograph provided in Fig. 6.7A as well as those presented in [1,3]. In the current experiments, cell distribution effects were limited by using relatively shallow scaffolds. However the problem could potentially be reduced further by modifying the aperture admittance model to account for layered biological media. Such models have been described in [5-8] but have not been popularly applied in dielectric spectroscopy. The complexity of the models for layered media is much greater and they are usually applied to material layers of evident contrasts in permittivity.

Two possible methods could be used to develop a layered media aperture admittance model for cell polymer constructs. The simpler approach, would be to assume the layer distribution of the sample and solve for the permittivity of each layer. Then, the EMA could be applied to calculate the cell concentration assumed in each layer producing an approximation of vertical cell distribution within the sample. The second approach, would be to choose a permittivity layer distribution

based on the best fit of the measurement to the aperture admittance model. The result could potentially be the best vertical cell distribution found within the scaffold. Fig. 7.2 illustrates how a scaffold could be broken down into layers of distinct cell distribution of distinct permittivity. However, it is possible that the layered model would be too complex to identify. Nonetheless, exploration of such models could be valuable to the system.

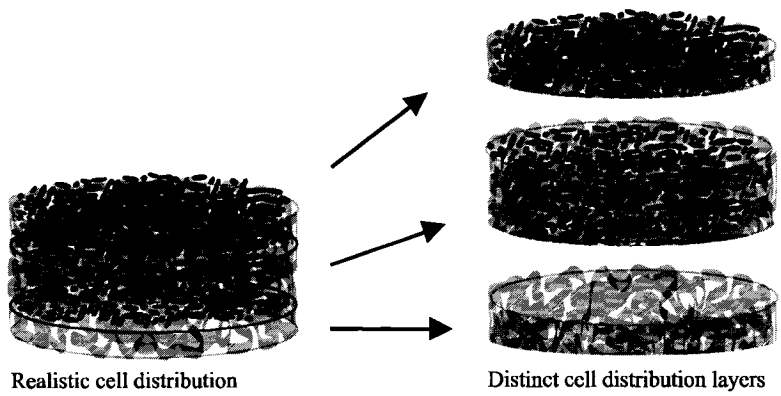

Figure 7.2. Stratified scaffold

Validation of this approximation could be performed by taking measurements from the top and bottom sides of the scaffold. The resulting permittivity layer distributions, for both proposed methods, should be reciprocals of each other. An elegant demonstration of the method's functionality would be to visually match a scanning electron micrograph of the transverse cut of a measured scaffold to the predicted vertical cell distribution.

7.1.2 Sample Modifications

There are numerous different types of scaffolds for tissue engineering applications as highlighted in the introductory chapters of this thesis. The scaffold and cell line used for this work were geared specifically towards bone engineering. To demonstrate, the range of the CPM system application, its efficacy should be demonstrated with different scaffold materials and cell lines.

Whatever the material of choice, it is imperative that the scaffold surface adhere well to the probe. Brittle and metallic scaffolds will not make good contact with the probe. Moreover, materials of high conductivity, such as metals, will disturb the permittivity measurement. Also, the measurement signal penetration depth in a new material should always be measured experimentally to assure significant sample representation.

Cell lines are pre-disposed to certain morphologies. Thus, the EMA should be modified accordingly. Any future work applying the EMA based on the loss factor as presented in this work to a cell-line of morphology other than lamellar will produce errors in the cell concentration measurement. Consequently, a general derivation for the EMA as a function of morphology is needed.

7.1.3 Cell Proliferation Kinetics

As previously reported the presence of ECM causes an underestimate of the cell concentration measurement within the scaffold. Thus, a study of the exact effect of ECM on the measured permittivity measurement is imperative to measure cell proliferation beyond the pre-tissue stage of seeded scaffold incubation. The modeling of how ECM effects permittivity would allow for its excision from the measurement improving cell concentration measure. In addition, an ECM model would allow for the ECM development within 3D scaffolds to be monitored and characterized, this is of interest, in itself since it is linked to mineralization and cell differentiation. The understanding of the ECM permittivity kinetics as related to cell concentration would produce further insight into the inner happenings of the 3D seeded scaffold.

The study of cell proliferation kinetics of various cell lines could lead to the optimization of their incubation environment. The effect of growth factors and their dosage on the cells could be explored and tailored accordingly. Resulting growth curves could be compared and analyzed to give insight into rates of tissue development.

Current 3D cell culture is the labor and time intensive stage of the tissue engineering paradigm. An understanding of the cell proliferation kinetics within

3D scaffolds based on the CPM system could lead to its use as a diagnostic device in the automation of 3D cell culture.

7.2 References

[1] P. O. Bagnaninchi, M. Dikeakos, T. Veres, and M. Tabrizian, "Monitoring of Stem Cell Proliferation and Differentiation using a Permittivity Responsive Biointerface," Materials Research Society Symposium Proceedings, vol. 773, pp. N7.12.1, 2003.

[12] P. O. Bagnaninchi, M. Dikeakos, T. Veres, and M. Tabrizian, "Towards On-Line Monitoring of Cell Growth in Microporous Scaffolds: Utilization and Interpretation of Complex Permittivity Measurements," Biotechnology and Bioengineering, vol. 84, pp. 343-350, 2003.

[13] P. O. Bagnaninchi, M. Dikeakos, T. Veres, and M. Tabrizian, "Complex Permittivity Measurement as a New Non-invasive Tool for Monitoring *In-vitro* Tissue Engineering and Cell Signature through the Detection of Cell Proliferation, Differentiation , and Pre-tissue Formation," IEEE Transactions on NanoBioscience, vol. 3, pp. 243-250, 2004.

[4] M. Sittinger, D. W. Hutmacher, and M. V. Risbud, "Current Strategies for Cell Delivery and Bone Regeneration," Current Opinion in Biotechnology, vol. 15, pp. 411-418, 2004.

[5] E. Alanen, T. Lahtinen, and J. Nuutinen, "Variational Formualtion of Open-Ended Coaxial Line in Contact with Layered Biological Medium," IEEE Transactions on Biomedical Engineering, vol. 45, pp. 1241-1248, 1998.

[6] D. K. Misra, "A Quasi-static Analysis of Open-ended Coaxial lines," IEEE Transactions on Microwave Theory and Technology, vol. MTT-35, pp. 925–928, 1987.

[7] S. Fan, K. Staebell, and D. Misra, "Static Analysis of an Open-Ended Coaxial Line Terminated by Layered Media," IEEE Transactions on Instrumentation and Measurement, vol. 39, pp. 435–437, 1990.

[8] S. Bakhtiari, S. I. Ganchev, and R. Zoughi, "Analysis of Radiation from an Open-Ended Coaxial Line into Stratified Dielectrics," IEEE Transactions on Microwave Theory and Technology, vol. 42, pp. 1261–1267,1994.

[9] L. S. Anderson, G. B. Gajda, and S. S. Stuchly, "Analysis of an Open-Ended Coaxial Line Sensor in Layered Dielectrics," IEEE Transactions on Instrumentation and Measurement, vol. IM-35, pp. 13-18, 1986.

APPENDIX A

Proceedings in IEEE Engineering in Medicine and Biology Society

---

A HIGHLY RESPONSIVE SYSTEM FOR ON-LINE *IN VITRO* ASSESSMENT OF TISSUE GROWTH WITHIN MICRO-POROUS POLYMER SCAFFOLDS

D. Dziong[1], P. Bagnaninchi[2], R.E. Kearney[1], M. Tabrizian[1]*

[1]McGill University, Montreal, Canada;

[2]Keele University, Keele, United Kingdom.

A.1 Abstract

We have proposed a highly responsive system for the on-line *in vitro* assessment of tissue growth within micro-porous polymer scaffolds that obviates any compromise of sample integrity. The system's function is based on the sample's loss factor: the imaginary part of the complex permittivity. Reflection measurements were performed using an open-ended coaxial probe and impedance analyzer; they were then related to the sample's complex permittivity by a quasi-static model of the probe's aperture admittance. Measurements of saline solutions showed that the real part of permittivity was corrupted by apparent polarization effects. Consequently, we developed a simplified formulation of the imaginary part of the Hanai-Wagner effective medium approximation to eliminate its dependence on the real part of complex permittivity measurement. This formulation allows the sample's cell concentration to be determined. The variation of a sample's cell concentration over time was used as a measure of tissue growth.

Measurements in the frequency range of 10 – 200 MHz were performed on micro-porous polymer scaffolds seeded with progressively greater number of cells. Results demonstrated that the system detected concentration differences between cell-seeded scaffolds

A.2 Introduction

The ultimate goal of tissue engineering is to produce a biological substitute *in vitro* that will restore tissue damaged, or lost, of trauma or disease [1]. The discipline's paradigm is to regenerate tissue by harvesting an autologous cell population, expanding it in culture, seeding it onto a scaffold, and cultivating it until ready for implantation [2].

Micro-porous polymer scaffolds are frequently used in tissue engineering applications because they have the favorable properties of malleability, high porosity, and a surface chemistry that allows cell attachment, proliferation, and differentiation [3]. Monitoring of constituent variation within seeded scaffolds is performed to diagnose levels of tissue formation. However, the present methods for determining tissue constituent variation in these scaffolds are time consuming, laborious, and often destructive [4,5].

In a previous work, we proposed a novel non-destructive method that used a complex permittivity (ϵ^*) measurement (CPM) as a means of monitoring cell differentiation and proliferation on-line in the relevant scaffold [6].

The application of CPM in tissue engineering has been largely limited to cell suspension measurements [7,8]. The extension of this method to monitor tissue growth within polymer scaffolds has allowed for a non-invasive evaluation of the inner-happenings of the cell-polymer construct. Indeed, the CPM method has been successful in determining the porosity of the scaffold, discriminating between different cell-lines, observing stem cell differentiation, and recording the change in cell concentration during the pre-tissue stage of incubation [6]. However, prolonged CPM monitoring of the cell-polymer construct revealed that the presence of significant cell side-product formation in the scaffold, particularly the extra-cellular matrix (ECM), can skew the cell concentration measurement.

To accurately quantify and model cell growth and the effect of ECM on the CPM it is desirable to increase the resolution of the system. A theoretical analysis of the cell concentration measurement revealed that measurements at lower frequencies would have greater sensitivity [6].

The CPM system is based on the reflective method of characterizing materials: permittivity is measured by obtaining the reflection coefficient at the sample interface. The system's five distinct elements are the focus of this work: (i) the cell-polymer matrix that acts as the bio-interface of the system, (ii) a biosensor that is an open-ended coaxial probe popularly applied in material characterization [9], (iii) a material analyzer that works in conjunction with the biosensor and extracts the reflection coefficient from the measurement, (iv) a mathematical model that relates the measured reflection coefficient to the permittivity of the sample, (v) an effective medium approximation (EMA) that acts as the sample's complex permittivity model. Proposed herein is a system tailored for lower frequency (10-200 MHz), greater sensitivity, non-destructive CPM.

A.3 Materials and Methods

A.3.1 Cell-polymer Matrix

The applied micro-porous polymer scaffold was primarily composed of chitosan – a partially deacytalated derivative of chitin, a polysaccharide. Chitosan has been applied for bone tissue engineering because it supports Osteoblast and Chondrocyte survival and phenotypic expression [10, 11].

Scaffolds were prepared by dissolving the high molecular Chitosan (Sigma Aldrich) at a 2% concentration in a water acetic mixture (1% v/v). The resulting gel was filtered into flasks and bathed in an ultra sonic bath to remove air bubbles. The gel was then cast in 24 well plates (15 mm diameter) and frozen at -20°C to generate an appropriate pore size [10]. Subsequently, the gels were lyophilized over three days. Once dry, each scaffold was carefully trimmed to obtain two samples slightly greater than a 3 mm high cylinder with uniform top and bottom surfaces. The scaffolds were neutralized and sterilized by immersion in progressively greater dilutions of ethanol (down to 70 %) [11].

Pre-osteoblast MC3T3-E1 subclone 14 (ATCC, USA) cell line was used as the cell model because it has been shown to attach well to the relevant porous

structures [6]. The cells were cultivated in alpha minimum essential medium, with L-glutamine and sodium bicarbonate at 2.5 g/L, supplemented with 10% foetal bovine serum and 1% penicillin streptomycin.

Then, a solution of specified cell concentration was prepared by means of a hemacytometer (Hausser Scientific) and carefully injected into the scaffold through a micro-liter tip. The resulting cell-polymer matrix was incubated at 37°C in an atmosphere of 100% humidity and 5% CO_2 for 6 hours.

A.3.2 Instrumentation

An open-ended coaxial probe (Agilent 85070D) was chosen as the biosensor for the CPM. The advantages of using a coaxial probe for material characterization have been widely acknowledged [9]. The most important advantages are: its simple and convenient geometry, the ability to perform measurements non-destructively over a frequency range of DC up to 50 GHz, and the elimination of tedious sample preparation [12]. The chosen probe had an electrical opening smaller than the thickness of the sample and less than half the sample's surface area (inner radius: a = 0.33 mm, outer radius: b = 1.5 mm); it was also terminated by a grounded conductive flange significantly greater than the sample (radius of 9.5 mm). These probe-to-sample dimension ratios facilitate modeling of the probe's aperture fields [13].

The applied material analyzer was an impedance analyzer (Agilent E4991A) that implements an RF I-V measurement method which has superior measurement sensitivity in the impedance range of biological materials than the reflection coefficient measurement produced by a network analyzer [14].

A.3.3 Reflection Model

A quasi-static model of the aperture's admittance related the sample's complex permittivity [9]:

$$Y_L = \frac{j2\omega\varepsilon_0\varepsilon^*}{\left[\ln\left(b/a\right)\right]^2}\left\{I_1 - \frac{k^2 I_2}{2}\right\} + \frac{k^3\pi\omega\varepsilon_0\varepsilon^*}{12}\left[\frac{b^2-a^2}{\ln\left(b/a\right)}\right]^2 \qquad \text{(A.1)}$$

where

$$k = \omega\sqrt{\varepsilon^* \varepsilon_0 \mu_0}, \tag{A,2}$$

$$I_1 = \int_{a}^{b}\int_{a}^{b}\int_{0}^{\pi} \frac{\cos(\phi)}{\sqrt{r^2 + r'^2 - 2rr'\cos(\phi)}} d\phi dr dr' \tag{A.3}$$

$$I_2 = \int_{a}^{b}\int_{a}^{b}\int_{0}^{\pi} \cos(\phi)\sqrt{r^2 + r'^2 - 2rr'\cos(\phi)}\, d\phi dr dr' \tag{A.4}$$

and where k is the wavenumber in the material medium, ϵ_0 and μ_0 are, respectively, the permittivity and permeability of free space. Also, a cylindrical coordinate system (r, ϕ, z) is assumed where primed coordinates represent the source points while unprimed ones represent the field points. The model requires only a single computation of its integrals per probe geometry allowing fast online performance. Furthermore, for low frequency measurements of materials with a high modulus of complex permittivity, such as biological tissue, only the first term of (A.1) is necessary [11]; which facilitates isolating the sample's permittivity:

$$\varepsilon^* = -j\frac{Y_L\left[\ln\left(b/a\right)\right]^2}{2\omega\varepsilon_0 I_1} \tag{A.5}$$

The probe's inherent length, the physical imperfections of the system and practical deviation from ideal assumptions produce errors in the reflection coefficient measurement. These errors are corrected by a calibration procedure based on a linear two-port network that de-embeds the true reflection coefficient [15]. The correction method requires the use of three calibration standards having well-described complex permittivity curves. We used air, a short circuit, and water – the complex permittivity of water was related by the Debye equation:

$$\varepsilon^*_{debye} = \varepsilon_\infty + \frac{\varepsilon_s - \varepsilon_\infty}{1 + j\omega\tau}. \tag{A.6}$$

The Debye parameters for water and other standard liquids: ε_s, ε_∞ and τ were taken from [12] and [16]. The admittance of water was then calculated by (A.1) and mapped to the reflection coefficient.

The model, as per (A.5), was tested with standard liquids having well-described complex permittivity curves: ethanol, methanol, saline solution of 0.1 normality (0.1 N), and saline solution of 0.3 normality (0.3 N). The accuracy of

the model was determined by calculating the percentage variance accounted for (VAF) defined as the square of the correlation coefficient (r).

The model was only significantly inaccurate in calculating the real part of saline solutions at low frequencies (Fig. A.1). The inaccuracy remained when the aperture admittance models from [17] and [18] were applied implying that the error was not model specific but rather a polarization effect that becomes more prevalent at low frequencies, specifically for electrolyte solutions. The closest theoretical dielectric spectrum approximation of cell medium is that of saline. In effect, an erroneous CPM of saline implies that the cell medium CPM is also related incorrectly. The problem was solved by modifying the EMA used to require only the imaginary part of the measurement as described below.

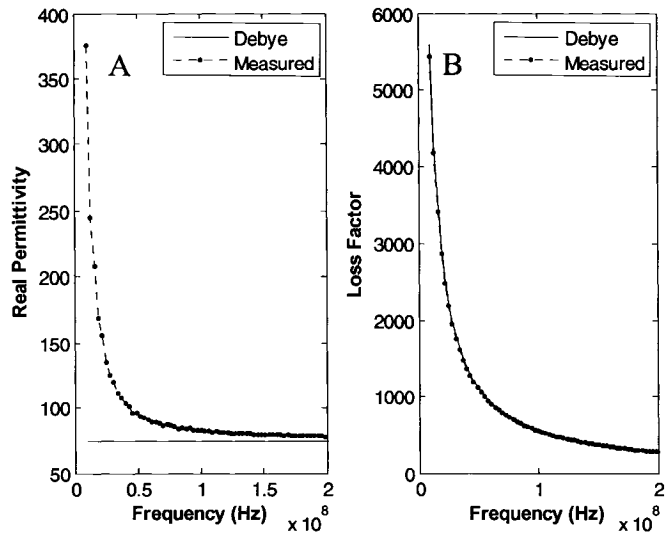

Figure A.1. Complex permittivity spectrum of saline (0.3 N) as measured and calculated by the Debye equation: (A) real part (VAF = 18.91 %), (B) imaginary part (VAF = 99.13 %).

A.3.4 Effective Medium Approximation

The Hanai-Wagner model [7] was implemented as the EMA to relate the CPM to the cell-polymer's constituents. The model is well suited for monitoring cell growth because it considers high volume fractions and includes a parameter (n) that can specify cell morphology. The model assumes all the cells to be composed of a low conducting membrane of fixed thickness (d_{mem}) filled with uniform cytosol; irrespective of assumed shape, the volume of the cell is related

by a parameter v = 1-(d_{mem}/r_{cell}) which assumes a spherical cell of radius (r_{cell}). Given the complex permittivity of the host medium (ϵ^*_m), the volume fraction of the cells (ϕ), cytosol's complex permittivity (ϵ^*_{cyt}), the real cell membrane permittivity (ϵ'_{mem}) and assuming a lamellar cell morphology (n = 1) for the attached cell the model produces an approximation of the effective medium's complex permittivity spectrum [6]:

$$\varepsilon^*_{eff} = \frac{\varepsilon^*_m \varepsilon^*_{cell}}{(1-\varphi)\varepsilon^*_{cell} + \varphi\varepsilon^*_m} \tag{A.7}$$

where

$$\varepsilon^*_{cell} = \frac{\varepsilon'_{mem}\varepsilon^*_{cyt}}{(1-v^3)\varepsilon^*_{cyt} + v^3\varepsilon'_{mem}}. \tag{A.8}$$

The imaginary component of the effective permittivity is a function of the cell volume fraction as described by (A.9); therefore, it alone is used to relate volume fraction change:

$$\mathrm{Im}\left[\varepsilon^*_{eff}(\omega)\right] = \frac{(\varepsilon'_{cell}\varepsilon''_m(1-\varphi)\varepsilon'_{cell}) + (\varepsilon''_{cell}\varepsilon'_m\varphi\varepsilon'_m) + (\varepsilon''_m\varepsilon''_{cell}(1-\varphi)\varepsilon''_{cell}) + (\varepsilon''_m\varepsilon''_{cell}\varphi\varepsilon''_m)}{((1-\varphi)\varepsilon'_{cell})^2 + (\varphi\varepsilon'_m)^2 + 2\varphi\varepsilon'_m(1-\varphi)\varepsilon'_{cell} + ((1-\varphi)\varepsilon''_{cell})^2 + (\varphi\varepsilon''_m)^2 + 2(\varphi\varepsilon''_m(1-\varphi)\varepsilon''_{cell})}. \tag{A.9}$$

An analysis of (A.9) revealed that it could be approximated by (A.10) given that $\varepsilon''^2_m, \varepsilon''^2_{cell} >> \varepsilon'^2_m$:

$$\mathrm{Im}\left[\varepsilon^*_{eff}(\omega)\right] = \frac{(1-\varphi)(\varepsilon'^2_{cell}\varepsilon''_m + \varepsilon''_m\varepsilon''^2_{cell}) + \varphi(\varepsilon''^2_m\varepsilon''_{cell})}{((1-\varphi)\varepsilon'_{cell})^2 + [(1-\varphi)\varepsilon''_{cell} + \varphi\varepsilon''_m]^2}. \tag{A.10}$$

The corresponding normalized error (Fig. A.2) shows that for the realistic range of volume fractions (ϕ < 0.3) the errors due to the approximation are less than 1 %. Consequently, the cell concentration can be determined without ever having to use the real part of CPM.

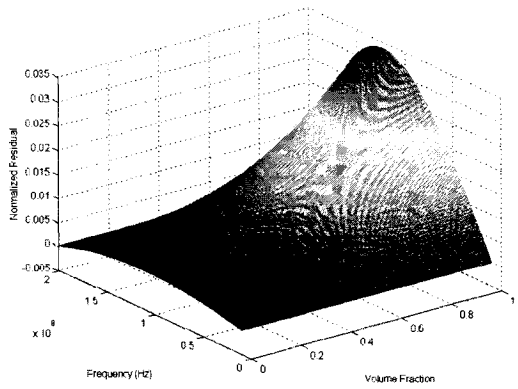

Figure A.2. The normalized error between (A.9) and (A.10) where the host medium is saline (0.3 N) as per (A.6) and the cell parameters are from [6].

The cell parameters involved were determined by fitting the imaginary CPM to (A.2). A non-linear fitting procedure implementing the trust region reflective-Newton algorithm was implemented to fit the data. The seed value and trust region of each cell parameter was set to the average and standard deviation of previously published data [6], respectively. Data fit analysis was performed for each loss factor measurement by calculating the normalized residuals and VAF.

A.3.5 Experimental Methods

As a preliminary test of the system's functionality and resolution, CPMs of scaffolds, seeded with incrementally greater number of cells, where performed in the low frequency range of 10-200 MHz with a frequency sampling period of 20 kHz. All experiments were performed under sterile conditions under a laminar flow-hood. Prior to measurement, samples were given time to settle to room temperature.

The CPM of 24 empty scaffolds immersed in medium was taken as the host medium measurement. The scaffolds were then divided into four sets and, respectively, seeded with 1 ml of 0.4, 0.45, 0.5, and 0.6 M cells/ml suspensions. The progressively incremental suspensions were to emulate cell proliferation. The resulting cell-polymer matrices were incubated for 6 hours to let the cells adhere to the scaffold. The sample was then centered on the probe, submerged in fresh medium, and three CPMs were performed.

A.4 Results and Discussion

Fig. A.3A shows a typical data fit of the loss factor measurement to (A.10). The presence of cells is characterized by a drop in the loss factor as highlighted by the Fig. A.3A insert. The loss factor is a function of conductivity; therefore, the low conducting cell membrane was expected to decrease the effective loss factor. The calculated VAF was always above 99 % while the normalized residuals where insignificant (less than 0.5 %) as depicted by Fig. A.3B. In effect, the loss factor EMA provided a good model for the sample.

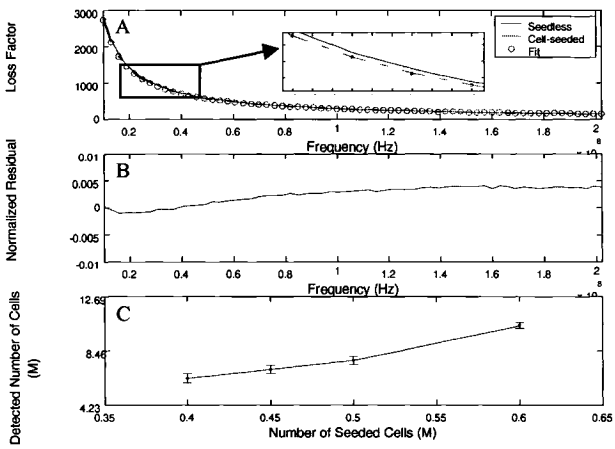

Figure A.3. Representative data for the loss factor measurement and fit: (A) measurement of seeded and seedless scaffold and corresponding fit (VAF = 99.99 %), (B) the average normalized residuals, (C) the extracted cell number from the four sets of scaffolds (r_{cell} = 10 μm).

Fig. A.3C shows the estimated cell numbers and demonstrates that they are overestimates of the hemacytometer cell count. As well, the recorded data trend was not linear as expected. The observed parameter inflation can be attributed to an inaccurate estimate of the cell model dimensions and the assumptions of the EMA. The nonlinearity of the trend was likely due to disproportionate cell adhesion, between the experiment's sets, to the polymer scaffold. Nonetheless, the relative trend of progressively increasing cell concentration was successfully recorded by the system.

A.5 Conclusion

A highly responsive CPM system has been proposed to non-destructively monitor tissue regeneration at frequencies of 10 – 200 MHz. As of yet, there is no widely accepted non-destructive, non-intrusive, method of monitoring tissue growth within micro porous scaffolds; our preliminary results exemplify the proposed system's function and application and have shown that the system can track cell concentration changes within a properly produced scaffold. We are extending our modeling and calibration methods to improve the estimates of the cell model parameters.

We believe that as the system becomes more robust the CPM method will become a useful measurement tool for tissue engineering.

A.6 Acknowledgments

This study was financially supported by the Fonds Quebecois de la Recherche sur la Nature et les Technologies (FQRNT). Agilent Technologies are greatly appreciated for their consultation and equipment loan.

A.7 References

[1] L. G. Griffith, and G. Naughton, "Tissue Engineering-Current Challenges and Expanding Opportunities," Science, vol. 295, pp. 1009-1016, 2002.

[2] J. J. Marler, J. Upton, R. Langer, and J. P.Vacanti, "Transplantation of Cells in Matrices for Tissue Regeneration," Advanced Drug Delivery Reviews, vol. 33, pp. 165-182, 1998.

[3] D. W. Hutmacher, "Scaffolds in Tissue Engineering Bone and Cartilage," Biomaterials, vol. 21, pp. 2529-2543, 2000.

[4] L. Olsson and J. Nielsen, "On-Line and *In situ* Monitoring of Biomass in Submerged cultivations," Trends in Biotechnology, vol. 15, pp. 517–522, 1997.

[5] G. Locher, B. Sonnleitner, and A. Fiechter, "On-line Measurement in Biotechnology: Techniques," Journal of Biotechnology, vol. 25, pp. 23–53, 1992.

[6] P. O. Bagnaninchi, M. Dikeakos, T. Veres, and M. Tabrizian, "Complex Permittivity Measurement as a New Non-invasive Tool for Monitoring *In-vitro* Tissue Engineering and Cell Signature Through the Detection of Cell Proliferation, Differentiation, and Pre-tissue Formation," IEEE Transactions on NanoBioscience, vol. 3, pp. 243-250, 2004.

[7] K. Asami, "Characterization of Biological Cells by Dielectric Spectroscopy," Journal of Non-Crystalline Solids, vol. 305, pp. 268-277, 2002.

[8] G. H. Markx, and C. L. Davey, "The Dielectric Properties of Biological Cells at Radiofrequencies: Applications in Biotechnology," Enzyme and Microbial Technology, vol. 25, pp. 161-171, 1999.

[9] C. L. Pournaropoulos, and D. K. Misra, "The Co-axial Aperture Electromagnetic Sensor and its Application in Material Characterization," Measurement Science and Technology, vol. 8, pp. 1191-1202, 1997.

[10] A. Lahiji, A. Sohrabi, D. S. Hungerford, and C. G. Frondoza, "Chitosan Supports the Expression of Extracellular Matrix Proteins in Human Osteoblasts and Chondrocytes," Biomedical Material Research, vol. 51, pp. 586-595, 2000.

[11] S. V. Madihally, and H. W. T. Matthew, "Porous Chitosan Scaffolds for Tissue Engineering," Biomaterials, vol. 20, pp. 1133-1142, 1999.

[12] C. L. Pournaropoulos, "A Study on the Coaxial Aperture Electromagnetic Sensor and its Application in Material Characterization" PhD dissertation, The University of Wisconsin-Milwaukee, 1996.

[13] D. D. Zutter, "Design Rules for an Experimental Setup Using an Open-Ended Coaxial Probe Based on Theoretical Modeling," IEEE Transactions on Instrumentation and Measurement, vol. 43, 1994.

[14] "Agilent Technologies Impedance Measurement Handbook" Agilent Technologies, 2003.

[15] J. Fitzpatrick, "Error Models for Systems Measurement," Microwave Journal, vol. 21, pp. 63-66, 1978.

[16] J. Dinebeditto and A. Uhlir, Jr., "Frequency Dependance of 50 Ω Coaxial Open-Circuit Reflection standard," IEEE Transactions on Instrumentation and Measurement, vol. IM-30, pp. 228-229, 1981.

[17] D. V. Blackham and R. D. Pollard, "An Improved Technique for Permittivity Measurements Using a Coaxial Probe," IEEE Transactions on Instrumentation and Measurement, vol. 46, pp. 1093-1099, 1997.

[18] M. A. Stuchly, M. Brady, S. Stuchly, and G. Gadja, "Equivalent Circuit of an Open-Ended Coaxial Line in a Lossy Dielectric," IEEE Transactions on Instrumentation and Measurement, vol. 31, pp. 116-119, 1982.

APPENDIX B
MATLAB Code

B.1 Cell Parameters

```
% This m-file acts as the main for the procedure of extracting
cell
% parameters. The function accepts the calibration (Ta12, Ts12,
Tw12),
% sample(Tmeas) and control (Tmeas2)reflection coefficient
measurements
% as well as the corresponding frequency vector (F).
% The function returns the cell signature and cell concentration.

function cell_sign = cells(Ta12, Ts12, Tw12,Tmeas, Tmeas2, F)

% the values of the Integrals related to the quasi-static
approximation % have been calculated by hand and stored in the
I1I2 matrix.

open  I1I2.mat
o  = ans;
I1 = o.I1I2.I1;
I2 = o.I1I2.I2;

% probe dimensions
a = 0.33/1000;
b = 1.5/1000;

% probe dielectric filling permittivity
er = 3.3;

% The theoretical reflection coefficient of water is calculated
cal = 2; % water
[TauS, yl, e_theo, ymodel] = theoTau(F,a,b,er,cal,I1,I2);

% The ideal Ts of the calibration standards:
% air reflection coeff
T1 = 1+j*0;

% liquid
T2 = TauS;

% short circuit
T3 = -1+j*0;

% de-embedd scaffold measurement
TauSample  = two_port_calib(F,Ta14,Tw14,Ts14,T1,T2,T3,Tmeas);

% de-embedd control measurement
TauControl = two_port_calib(F,Ta14,Tw14,Ts14,T1,T2,T3,Tmeas2);

% map reflection coefficient into admittance
```

```
ysample = (1-TauSample)./(1+TauSample);

% map reflection coefficient into admittance
ycontrol = (1-TauControl)./(1+TauControl);

% calculate the permittivity of the measurement
e_sample  = model_1(ysample, F, a, b, I1, I2);
e_control = model_1(ysample, F, a, b, I1, I2);

% Measurement are usually performed over a frequency greater then
that
% of interest. The following parameters are chosen to match the
indexes
% of the desired frequency range.

LFmin = 1;
LFmax = 65;

freq_LF      = freq_part(LFmin, LFmax, F);
e_sampleLF   = freq_part(LFmin, LFmax,  e_sample);
e_controlLF  = freq_part(LFmin, LFmax,  e_control);

% cell model parameters
d = 0.1;            % shell thickness
R = 10;             % outer diameter of the shell
v = (1-0.01/10)^3;  % thickness-radius relationship of the cell

choice = 0;         % choice: 0 or 1, decides the method for lsqnl

% Choice zero allows for limiting the constituent range (this is
the
% method applied for presented results)

if choice==0
    options =
optimset('LargeScale','on','MaxFunEvals',100000,'Display','on','To
lFun',0.0000000001,'MaxIter',15000);

% lower limit for: membrane permittivity, cytosol perm, cytoplasm
% conductivity, volume fraction
    lower = [10 30 0.1 0];

% upper limit for: membrane permittivity, cytosol perm, cytoplasm
% conductivity, volume fraction
    upper = [60 90 2 0.9];
end

% choice one does not limit the value of the constituents
if choice==1
    options =
optimset('LargeScale','off','MaxFunEvals',100000,'Display','on','T
olFun',0.00000001,'MaxIter',15000);
    lower = [];
    upper =[];
end

% starting guesses (based on literature and Pierres work):
```

```
g1 = 3;      % membrane real permittivity
g2 = 11;     % cytoplasm real part of permittivity
g3 = 1;      % cytoplasm conductivity
g4 = 0.01    % volume fraction

% store guesses as a vector
guesses = [g1,g2,g3,g4]
% perform fit.
[xLF,ResnormLF,FVALLF,EXITFLAGLF,OUTPUTLF,LAMBDALF,JACOBLF]=
lsqnonlin('HanaiWagner_Fit_im',guesses,lower,upper,options,freq_LF
, e_sampleLF,e_controlLF);

cell_sign = xLF;
```

B.1.1 Function to Minimize

```
% The function accepts:
% The guesses for the cell parameters (guess)
% The frequency vector (Freq)
% The seeded scaffold permittivity (Es)
% The control scaffold permittivity (Em)
% The function returns the difference between sample model and
measurement

function SS = HanaiWagner_Fit_im(guess, Freq, Es, Em)

% membrane real permitivity
er_mem = guess(1);

% cytosol real permitivity
er_cyt = guess(2);

% cytosol conductivity
k_cyt = guess(3);

% volume fraction
phi = guess(4);

w = 2*pi.*Freq;

eo = 8.8542*10^-12;

% membrane conductivity
k_mem = 0;
% membrane thickness
d_mem = 0.01;

% membrane permittivity
e_mem = er_mem - i.*k_mem./(2*pi*eo.*Freq);

% Outer diameter of cell (we are assuming spherical shape for
volume)
R_cyt = 10;

% cytosol permittivity
e_cyt = er_cyt -i.*k_cyt./(2*pi*eo*Freq);
```

```
%  volume parameter
v = (1-d_mem/R_cyt)^3;

%  cell permittivity
e_cell = (er_mem.*e_cyt)./(((1-v).*e_cyt)+(v.*er_mem));

emr = real(Em);
emi = imag(Em);

ecr = real(e_cell);
eci = imag(e_cell);

% The imaginary formulation
ei = ((((ecr.*emi)+(eci.*emr)).*(((1-phi).*ecr)+(phi.*emr)))-
((emr.*ecr-eci.*emi).*((1-phi).*eci+phi.*emi))./...
    ((((1-phi).*ecr)+(phi.*emr)).^2+(((1-
phi).*eci)+(phi.*emi)).^2);

e_eff_c = ei;

e_eff_c = e_eff_c - (imag(Es));

% get the length of the vector
L=length(Freq);

%  Store the real part of the function to be minimized in the
first half
%  of the vector
SS(1:L)=real(e_eff_c);
```

B.1.2 Two Port Network

```
% Given three measured calibration standards and their ideal
reflection
% coefficients and a measured reflection coefficient of the
current
% sample the function returns the de-embedded reflection
coefficient as
% per a two-port network model.

function Tau = two_port_calib(T1m,T2m,T3m,Tmeas,T1,T2,T3,F)

% T with m corresponds to measured reflection coeff values.
% T without m corresponds to the ideal reflection coeff values.

S11 = ((T1.*T2.*T3m.*(T1m-T2m)) + (T2.*T3.*T1m.*(T2m-T3m)) +
(T3.*T1.*T2m.*(T3m-T1m)))./ ((T1.*T2.*(T1m-T2m)) + (T2.*T3.*(T2m-
T3m)) + (T3.*T1.*(T3m-T1m)));

S22 = (T3.*(S11-T2m)+T2.*(T3m-S11))./(T2.*T3.*(T3m-T2m));

S12S21 = ((T2m-S11).*(1-S22.*T2))./T2;

delta = S11.*S22 - S12S21;
```

```
Tau = (Tmeas - S11) ./ (Tmeas.*S22 - delta);
```

B.1.3 Inverse Problem with Quasi-Static Approximation

```
% function accepts:
% the measured admittance yl
% the corresponding frequency F
% the dimensions of the applied coaxial probe a and b
% the solved for integrals of the quasi static equation I1 and I2
% the function returns the sample complex permittivity

function e = model_1(yl, F, a, b, I1, I2)

yc = 1/50;

uo = 4*pi*(10^-7);
eo = (10^-9)/(36*pi);
w  = 2*pi.*F;

n1 = (j.*2.*w.*eo);
n2 = log(b/a)^2;
yl = yl*yc;
e  = yl./((n1./n2)*I1);
```

5. RESEARCH PERSONNEL: (attach additional sheets if preferred)

Name	Department	Job Title/Classification	Trained in the safe use of biological safety cabinets within the last 3 years? If yes, indicate training date.
Lucie Marcotte	BMED	Research associate	No.
Jean-Philippe St-Pierre	BMED	Master student	No
Cyrille Fleury	BMED	Master student	No
Line Mongeon	BMED	Technician	No
Kim Douglas	BMED	PhD student	No
Shahabeddin Faghihi	BMED	PhD student	No

6. Briefly describe:

i) the biohazardous material involved (e.g. bacteria, viruses, human tissues, toxins of biological origin) & designated biosafety risk group

bacteria, cell lines (mammalian)
↳ E. coli (non-pathogenic)

ii) the procedures involving biohazards

cell and bacterial culture

iii) the protocol for decontaminating spills

as requested by McGill - ethanol, detergent, bleach disinfection

7. Does the protocol present conditions (e.g. handling of large volumes or high concentrations of pathogens) that could increase the hazards?

no

5. RESEARCH PERSONNEL (continued)			
Name	Department	Job Title / Classification	Trained in the safe use of biological safety cabinets within the last 3 years? If yes, indicate training date.
Shawn Carrigan	BMED	PhD student	No
Dariusz Dziong	BMED	Master student	No
Mylène Gravel	BMED	Master student	No
Manuela Mandu	BMED	PhD student	No
Cathy Tkaczyk	BMED	PhD student	No
Anna Hillberg	BMED	Post doctoral fellow	No

8. Do the specific procedures to be employed involving genetically engineered organisms have a history of safe use?

~~no~~ N/A

9. What precautions will be taken to reduce production of infectious droplets and aerosols?

~~n/a~~ Manipulation of cultures will be carried out in a BSC

10. Will the biohazardous materials in this project expose members of the research team to any risks that might require special training, vaccination or other protective measures? If yes, please explain.

no

11. Will this project produce combined hazardous waste – i.e. radioactive biohazardous waste, biohazardous animal carcasses contaminated with toxic chemicals, etc.? If yes, please explain how disposal will be handled.

no

12. List the biological safety cabinets to be used.

Building	Room No.	Manufacturer	Model No.	Serial No.	Date Certified
Lyman Duff	323	microzone	BK-2-4	801-4534	14/05/04